

1 Can assimilation of crowdsourced data in hydrological 2 modelling improve flood prediction?

3

4 M. Mazzoleni¹, M. Verlaan², L. Alfonso¹, M. Monego³, D. Norbiato³, M. Ferri³ and D.P.
5 Solomatine^{1,4}

6 [1]{UNESCO-IHE Institute for Water Education, Delft, The Netherlands}

7 [2]{Deltares, Delft, The Netherlands}

8 [3]{Alto Adriatico Water Authority, Venice, Italy}

9 [4]{Delft University of Technology, Water Resources Section, Delft, The Netherlands}

10 Correspondence to: M. Mazzoleni (m.mazzoleni@unesco-ihe.org)

11

12 **Abstract**

13 Monitoring stations have been used for decades to properly measure hydrological variables and
14 better predict floods. To this end, methods to incorporate these observations into mathematical
15 water models have also been developed. Besides, in recent years the continued technological
16 advances, in combination with the growing inclusion of citizens in participatory processes
17 related to water resources management, have encouraged the increase of citizen science projects
18 around the globe. In turn, this has stimulated the spread of low-cost sensors to allow citizens to
19 participate in the collection of hydrological data in a more distributed way than the classic static
20 physical sensors do. However, two main disadvantages of such crowdsourced data are the
21 irregular availability and variable accuracy from sensor to sensor, which makes them
22 challenging to use in hydrological modelling. This study aims to demonstrate that streamflow
23 data, derived from crowdsourced water level observations, can improve flood prediction if
24 integrated in hydrological models. Two different hydrological models, applied to four case
25 studies, are considered. Realistic (albeit synthetic) time series are used to represent
26 crowdsourced data in all case studies. In this study it is found that the data accuracies has much
27 more influence on the model results than the irregular frequencies of data availability at which
28 the streamflow data is assimilated. This study demonstrates that data collected by citizens,

29 characterised by being asynchronous and inaccurate, can still complement traditional networks
30 formed by few accurate, static sensors and improve the accuracy of flood forecasts.

31 **1 Introduction**

32 Observations of hydrological variables measured by physical sensors have been increasingly
33 integrated into mathematical models by means of model updating methods. The use of these
34 techniques allows for the reduction of intrinsic model uncertainty and improves the flood
35 forecasting accuracy (Todini et al., 2005). The main idea behind model updating techniques is
36 to either update model input, states, parameters or outputs as new observations become
37 available (Refsgaard, 1997; WMO, 1992). Input update is the classical method used in
38 operational forecasting and uncertainties of the input data can be considered as the main source
39 of uncertainty of the model (Bergström, 1991; Canizares et al., 1998; Todini et al., 2005).
40 Regarding the state updating, filtering methods as Kalman filter (Kalman, 1960), extended
41 Kalman filter (Aubert et al., 2003; Madsen and Cañizares, 1999; Verlaan, 1998), Ensemble
42 Kalman filter (Evensen, 2006) and Particle filter (Weerts and El Serafy 2006) are the most used
43 approaches to update a model when new observations are available.

44 Due to the complex nature of the hydrological processes, spatially and temporally distributed
45 measurements are needed in the model updating procedures to ensure a proper flood prediction
46 (Clark et al., 2008; Mazzoleni et al., 2015; Rakovec et al., 2012). However, traditional physical
47 sensors require proper maintenance and personnel, which can be cost prohibitive for a vast
48 network. For this reason, improvements to monitoring technology have led to the spread of low-
49 cost sensors to measure hydrological variables, such as water level or precipitation, in a more
50 distributed way. The main advance of using these type of sensors, defined in the paper as a
51 “social sensor”, is that they can be used not only by technicians but also by regular citizens and
52 that due to their reduced cost and voluntary labor by citizens, result in a more spatially
53 distributed coverage. The idea of designing these alternative networks of low-cost social
54 sensors and using the obtained crowdsourced observations is the base of the European Project
55 WeSenseIt (2012-2016) and various other projects that proposed to assess the usefulness of
56 crowdsourced observations inferred by low-cost sensors owned by citizens. For instance, in the
57 project CrowdHydrology (Lowry and Fienen, 2013), a method to monitor stream stage at
58 designated gauging staffs using crowdsource-based text messages of water levels is developed
59 using untrained observers. Cifelli et al. (2005) described a community-based network of

60 volunteers (CoCoRaHS), engaged in collecting precipitation measurements of rain, hail, and
61 snow. An example of hydrological monitoring, established in 2009, of rainfall and streamflow
62 values within the Andean ecosystems of Piura, Peru, based on citizen observations is reported
63 in Célleri et al. (2009). Degrossi et al. (2013) used a network of wireless sensors in order to
64 map the water level in two rivers passing by Sao Carlos, Brazil. Recently, the iSPUW Project
65 was initiated to integrate data from advanced weather radar systems, innovative wireless
66 sensors, and crowdsourcing of data via mobile applications, in order to better predict flood
67 events the Dallas-Fort Worth Metroplex urban water systems (ISPUW, 2015; Seo et al., 2014).
68 Other examples of crowdsourced water-related information include the so-called Crowdmap
69 platform for collecting and communicating the information about the floods in Australia in 2011
70 (ABC, 2011), and informing citizens about the proper time for water supply in an intermittent
71 water system (Alfonso, 2006; Au et al., 2000; Roy et al., 2012). Wehn et al. (2015) stressed the
72 importance and need of public participation in water resources management to ensure citizens'
73 involvement in the flood management cycle. Buytaert et al. (2014) provide a detailed and
74 interesting review of the examples of citizen science applications in hydrology and water
75 resources science. In this review paper, the potential of citizen science, based on robust, cheap,
76 and low-maintenance sensing equipment, to complement more traditional ways of scientific
77 data collection for hydrological sciences and water resources management is explored.

78 The traditional hydrological observations from physical sensors have a well-defined structure
79 in terms of frequency and accuracy. On the other hand, crowdsourced observations are provided
80 by citizens with varying experience of measuring environmental data and little connections
81 between each other, and the consequence is that the low correlation between the measurements
82 might be observed. So far, in operational hydrology practice, the added value of crowdsourced
83 data it is not integrated into the forecasting models but only used to compare the model results
84 with the observations in a post-event analysis. This can be related to the intrinsic variable
85 accuracy, due to the lack of confidence in the data quality from these heterogeneous sensors,
86 and the variable life-span of the crowdsourced observations.

87 Regarding data quality, Bordogna et al. (2014) and Tulloch and Szabo (2012) stated that quality
88 control mechanisms should consider contextual conditions to deduce indicators about reliability
89 (the expertise level of the crowd), credibility (the volunteer group), and performance of
90 volunteers as they relate to accuracy, completeness and precision level. Bird et al. (2014)
91 addressed the issue of data quality in conservation ecology by means of new statistical tools to

92 assess random error and bias. Cortes et al. (2014) evaluated data quality by distinguishing the
93 in-situ data collected between volunteers and technicians and comparing the most frequent
94 value reported at a given location. With in-situ exercises, it might be possible to have an
95 indication of the reliability of data collected. However, this approach is not enough at an
96 operational level to define accuracy in data quality. For this reason, to estimate observation
97 accuracy in real-time, one possible approach could be to filter out the measurements following
98 a geographic approach which defines semantic rules governing what can occur at a given
99 location (e.g. Vandecasteele and Devillers, 2013). Another approach could be to compare
100 measurements collected within a predefined time-window in order to calculate the most
101 frequent value, the mean, and the standard deviation.

102 Crowdsourced observations can be defined as *asynchronous* because they do not have
103 predefined rules about the arrival frequency (the observation might be taken once, occasionally
104 or at irregular time steps, which can be smaller than the model time step) and accuracy of the
105 measurement. In a recent paper, Mazzoleni et al. (2015) presented results of the study of the
106 effects of distributed synthetic streamflow observations having synchronous intermittent
107 temporal behavior and variable accuracies in a semi-distributed hydrological model. It was
108 shown that the integration of distributed uncertain intermittent observations with single
109 measurements coming from physical sensors would allow for the further improvements in
110 model accuracy. However, it was not considered the possibility that the asynchronous
111 observations might be coming at the moments not coordinated with the model time steps. A
112 possible solution to handle asynchronous observations in time with Ensemble Kalman Filter
113 (EnKF) is to assimilate them at the moments coinciding with the model time steps (Sakov et
114 al., 2010). However, as these authors mention, this approach requires the disruption of the
115 ensemble integration, the ensemble update and a restart, which may not be feasible for large-scale
116 forecasting applications. Continuous assimilation approaches, such as three-dimensional and four-
117 dimensional variational methods (3D-Var and 4D-Var), are usually implemented in oceanographic
118 modeling in order to integrate asynchronous observations at their corresponding arrival moments
119 (Derber and Rosati, 1989; Huang et al., 2002; Macpherson, 1991; Ragnoli et al., 2012). In fact,
120 oceanographic observations are commonly collected at asynchronous times. For this reason, in
121 variational data assimilation, the past asynchronous observations are simultaneously used to
122 minimize the cost function that measures the weighted difference between background states
123 and observations over the time interval, and identify the best estimate of the initial state
124 condition (Drecourt, 2004; Ide et al., 1997; Li and Navon, 2001). In addition to the 3D-Var and

125 4D-Var methods, Hunt et al. (2004) proposed a Four Dimensional Ensemble Kalman Filter
126 (4DEnKF) which adapts EnKF to handle observations that have occurred at non-assimilation
127 times. Furthermore, for linear dynamics, 4DEnKF is equivalent to the instantaneous
128 assimilation of the measured data (Hunt et al., 2004). Similarly to 4DEnKF, Sakov et al. (2010)
129 proposed a modification of the EnKF, the Asynchronous Ensemble Kalman Filter (AEnKF), to
130 assimilate asynchronous observations (Rakovec et al., 2015). Contrary to the EnKF, in the
131 AEnKF current and past observations are simultaneously assimilated at a single analysis step
132 without the use of an adjoint model. Yet another approach to assimilate asynchronous
133 observations in models is the so-called First-Guess at the Appropriate Time (FGAT) method.
134 Like in 4D-Var, the FGAT compares the observations with the model at the observation time.
135 However, in FGAT the innovations are assumed constant in time and remain the same within
136 the assimilation window (Massart et al., 2010). In light of reviewed approaches, this study uses
137 a pragmatic method, due in part to the linearity of the hydrological models implemented in this
138 study, to assimilate the asynchronous crowdsourced observations.

139 The main objective of this study is to assess the potential use of crowdsourced data within
140 hydrological modeling. In particular, the specific objectives of this study are a) to assess the
141 influence of different arrival frequencies and accuracies of crowdsourced data from a single
142 social sensor on the assimilation performances, and b) to integrate distributed low-cost social
143 sensors with a single physical sensor to assess the improvement in the streamflow prediction in
144 an early warning system. The methodology is applied in the Brue (UK), Sieve (Italy), Alzette
145 (Luxemburg) and Bacchiglione (Italy) catchments, considering lumped and semi-distributed
146 hydrological models respectively. Synthetic time series, asynchronous in time and with random
147 accuracies, that imitate the crowdsourced data, are generated and used.

148 The study is organized as follows. Firstly, the case studies, the crowdsourced data and the
149 datasets used are presented. Secondly, the hydrological models, the procedure used to integrate
150 the crowdsourced data and the set of experiments are reported. Finally, the results, discussion,
151 and conclusions are presented.

152 **2 Sites locations and data**

153 **2.1 Case studies**

154 Four different case studies are used to validate the obtained results for areas having diverse
155 topographical and hydrometeorological features and represented by two different hydrological
156 models. The Brue, Sieve, and Alzette catchments are considered because of the availability of
157 precipitation and streamflow data, while the Bacchiglione catchment is one of the official case
158 studies of the WeSenseIt Project (Huwald et al., 2013).

159 **2.1.1 Brue catchment**

160 The first case study is located in the Brue catchment (Figure 1), in Somerset, with a drainage
161 area of about 135 km² at the catchment outlet in Lovington. The SRTM DEM of 90m resolution
162 is used to derive the topographical characteristics, streamflow network and the consequent time
163 of concentration, by means of the Giandotti equations (Giandotti, 1933), which is about 10 h.
164 The hourly precipitation (49 rainfall stations) and streamflow data used in this study are
165 supplied by the British Atmospheric Data Centre from the HYREX (Hydrological Radar
166 Experiment) project (Moore et al., 2000; Wood et al., 2000). The average precipitation value in
167 the catchment is estimated using the Ordinary Kriging (Matheron, 1963).

168 **2.1.2 Sieve catchment**

169 The second case study is the Sieve catchment (Figure 1), a tributary of the Arno River, located
170 in the Central Italian Apennines, Italy. The catchment has a drainage area of about 822km² with
171 the length of 56 km and it covers mostly hills and mountainous areas with an average elevation
172 of 470 m above sea level. The time of concentration of the Sieve catchment is about 12 h.
173 Hourly streamflow data are provided by the Centro Funzionale di Monitoraggio Meteo
174 Idrologico-Idralico of the Tuscany Region at the outlet section of the catchment at Fornacina.
175 The mean areal precipitation is calculated by Thiessen polygon method using 11 rainfall
176 stations (Solomatine and Dulal, 2003).

177 **2.1.3 Alzette catchment**

178 The Alzette catchment is located in the large part of the Grand-Duchy in Luxembourg. The
179 drainage area of the catchment is about 288 km² and the river has a length of 73 km along
180 France and Luxembourg. The catchment covers cultivated land, grassland, forestland and

181 urbanized land (Fenicia et al., 2007). Thiessen polygon method is used for averaging the series
182 at the individual stations and calculate hourly rainfall series (Fenicia et al., 2007), while
183 streamflows data are available measured at the Hesperange gauging station.

184 **2.1.4 Bacchiglione catchment**

185 The last case study is the upstream part of the Bacchiglione River basin, located in the North-
186 East of Italy, and tributary of the Brenta River which flows into the Adriatic Sea at the South
187 of the Venetian Lagoon and at the North of the Po River delta. The study area has an overall
188 extent and river length of about 400 km² and 50 km (Ferri et al., 2012). The main urban area
189 located in the downstream part of the study area is Vicenza. The analysed part of the
190 Bacchiglione River has three main tributaries. On the Western side is the confluences with the
191 Bacchiglione are the Leogra and the Orolo Rivers, while on the Eastern side there is the
192 Timonchio River (see Figure 2). The Alto Adriatico Water Authority (AAWA) has
193 implemented an Early Warning System to forecast the possible future flood events.

194 **2.2 Crowdsourced data**

195 Social sensors can be used by citizens to provide crowdsourced distributed hydrological
196 observations such as precipitation and water level. An example of these sensors can be a staff
197 gauge, connected to a QR code, on which citizens can read water level indication and send
198 observations via a mobile phone application. Another example is the collection of rainfall data
199 via lab-generated videos (Alfonso et al., 2015). Recently, within the activities of the WeSenseIt
200 Project (Huwald et al., 2013), one physical sensor and three staff gauges complemented by a
201 QR code were installed in the Bacchiglione River to measure the water level. In particular, the
202 physical sensor is located at the outlet of the Leogra catchment while the three social sensors
203 are located at the Timonchio, Leogra and Orolo catchments outlet respectively (see Figure 2).

204 It is worth noting that, in most of the cases, it is difficult to directly assimilate water level
205 observations within hydrological models. However, it is highly unrealistic to assume that
206 citizens might observe streamflow directly. For this reason, crowdsourced *observations* of
207 water level are used to calculate crowdsourced *data* (CSD) of streamflow, by means of rating
208 curves assessed for the specific river location, which can be easily assimilated into hydrological
209 models. It is because of both the uncertainty in rating curve estimation at the social sensor
210 location and the error in the water level measurements that CSD have such low and variable
211 accuracies when compared to streamflow data estimated from classic physical sensors. CSD is

212 then assimilated within mathematical models as described in Figure 3 (“Overall information
213 flow”).

214 In most hydrological applications, streamflow data from physical sensors are derived (and
215 integrated into hydrological models) at a regular, synchronous, time steps. In contrast,
216 crowdsourced water level observations are obtained by diverse type of citizens at random
217 moments (when a citizen decides to send data). Thus, from the modeling viewpoint CSD have
218 three main characteristics: a) irregular arrival frequency (asynchronicity); b) random accuracy;
219 and c) random number of CSD received within two model time steps. Because streamflow CSD
220 are not available in the case studies at the moment of this study, realistic synthetic CSD with
221 these characteristics are generated (“Considered information flow” in Figure 3).

222 For the Brue, Sieve and Alzette catchments observed hourly streamflow data at the catchments
223 outlet are interpolated to represent CSD coming at arrival frequencies higher than hourly. For
224 the Bacchiglione catchment, synthetic hourly CSD of streamflow are calculated using measured
225 precipitation recorded during the considered flood events (post-event simulation) as input in
226 the hydrological model of the Bacchiglione catchment. A similar approach, termed “observing
227 system simulation experiment” (OSSE), is commonly used in meteorology to estimate synthetic
228 “true” states and measurements by introducing random errors in the state and measurement
229 equations (Arnold and Dey, 1986; Errico et al., 2013; Errico and Privé, 2014). OSSEs have the
230 advantage of making it possible to compare estimates to “true” states and they are often used
231 for validating the data assimilation algorithms.

232 Further details and assumptions regarding the characteristics of CSD and related uncertainty
233 are provided in the next sections.

234 **2.3 Datasets**

235 Three flood events for each one of the four described catchments are considered to assess the
236 assimilation of CSD in hydrological modeling.

237 For the Brue catchment, a 2 years’ time series (June 1994 to May 1996) of observed streamflow
238 and precipitation data are available for model calibration and validation. On the other hand, for
239 the Sieve catchment only 3 months of hourly runoff, streamflow and precipitation data
240 (December 1959 to February 1960) are available (Solomatine and Shrestha, 2003). For the
241 Alzette catchment, two-year hourly data (July 2000 to June 2002) are used for the model
242 calibration and validation (Fenicia et al., 2007). For these catchments, the observed

243 precipitation values are treated as the “perfect forecasts” and are fed into the hydrological
244 model.

245 For the Bacchiglione catchment, three flood events occurred in 2013, 2014 and 2016 are
246 considered. In particular, the one of 2013 had high intensity and resulted in several traffic
247 disruptions at various locations upstream Vicenza. The forecasted time series of precipitation
248 (3-days weather forecast) is used as input to the hydrological model. In all the case studies, the
249 observed values of streamflow at the catchment outlet (Ponte degli Angeli for the Bacchiglione)
250 are used to assess the performance of the hydrological model.

251 **3 Methodology**

252 **3.1 Hydrological modelling**

253 **3.1.1 Lumped model**

254 A lumped conceptual hydrological model is implemented to estimate the streamflow
255 hydrograph at the outlet section of the Brue, Sieve and Alzette catchments. The choice of the
256 model is based on previous studies performed on the Brue catchment (Mazzoleni et al., 2015).
257 Direct runoff is the input in the conceptual model and it is assessed by means of the Soil
258 Conservation Service Curve Number method (Mazzoleni et al., 2015). The average Curve
259 Number value within the catchment is calibrated by minimizing the difference between the
260 simulated volume and observed quickflow, using the method proposed by Eckhardt (2005), at
261 the outlet section.

262 The main module of the hydrological model is based on the Kalinin-Milyukov-Nash (KMN),
263 Szilagyi and Szollosi-Nagy (2010), equation:

$$264 \quad Q_t = \frac{1}{k} \cdot \frac{1}{(n-1)!} \int_{t_0}^t \left(\frac{\tau}{k}\right)^{n-1} \cdot e^{-\tau/k} \cdot I(t-\tau) \cdot d\tau \quad (1)$$

265 where I is the model forcing (in this case direct runoff), n (number of storage elements) and k
266 (storage capacity expressed in hours) are the two model parameters and Q is the model output
267 (streamflow in m^3/s). In this study, the parameter k is assumed as a linear function between the
268 time of concentration and a coefficient c_k . The discrete state-space system of Eq. (1) derived by

269 Szilagyi and Szollosi-Nagy (2010) is used in this study to apply the data assimilation approach
270 (Mazzoleni et al., 2015, 2016).

271 The model calibration is performed maximizing the Nash-Sutcliffe efficiency (N_{SE}) and the
272 correlation between the simulated and observed value of streamflow, at the outlet point of the
273 Brue, Sieve and Alzette catchments, using historical time series. The results of the calibration
274 provided a value of the parameters n and c_k equal to 4 and 0.026, 1 and 0.0055, and 1 and
275 0.00064 for the Brue, Sieve, and Alzette catchments respectively.

276 3.1.2 Semi-distributed model

277 The hydrological and routing models used in this study are based on the early warning system
278 implemented by the AAWA and described in Ferri et al. (2012). One of the goals of this study,
279 in the framework of the WeSenseIt Project, is to test our methodology using synthetic CSD in
280 the existing early warning system of the Bacchiglione catchment.

281 In the schematization of the Bacchiglione catchment, the location of physical and social sensors
282 corresponds to the outlet section of three main sub-catchments, Timonchio, Leogra and Orolo,
283 while the remaining sub-catchments are considered as inter-catchment. For both sub-
284 catchments and inter-catchments, a conceptual hydrological model, described below, is used to
285 estimate the outflow (streamflow) hydrograph. The streamflow hydrograph of the three main
286 sub-catchments is considered as upstream boundary conditions of a routing model used to
287 propagate the flow up to the catchment outlet (see Figure 2), while the outflow from the inter-
288 catchment is considered as an internal boundary condition to account for their corresponding
289 drained area. In the following, a brief description of the main components of the hydrological
290 and routing models is provided.

291 The input for the hydrological model consists of precipitation only. The hydrological response
292 of the catchment is estimated using a hydrological model that considers the routines for runoff
293 generation and a simple routing procedure. The processes related to runoff generation (surface,
294 sub-surface and deep flow) are modeled mathematically by applying the water balance to a
295 control volume representative of the active soil at the sub-catchment scale. The water content
296 S_w in the soil is updated at each calculation step dt using the following balance equation:

$$297 \quad S_{w,t+dt} = S_{w,t} + P_t - R_{sur,t} - R_{sub,t} - L_t - E_{T,t} \quad (2)$$

298 where P and E_T are the components of precipitation and evapotranspiration, while R_{sur} , R_{sub} and
 299 L are the surface runoff, sub-surface runoff and deep percolation model states respectively (see
 300 Figure 2). The surface runoff R_{sur} is expressed by the equation based on specifying the critical
 301 threshold beyond which the mechanism of dunnian flow (saturation excess mechanism)
 302 prevails:

$$303 \quad R_{\text{sur},t} = \begin{cases} C \cdot \left(\frac{S_{w,t}}{S_{w,\text{max}}} \right) \cdot P_t \Rightarrow P_t \leq f = \frac{S_{w,\text{max}} \cdot (S_{w,\text{max}} - S_{w,t})}{(S_{w,\text{max}} - C \cdot S_{w,t})} & \\ P_t - (S_{w,\text{max}} - S_{w,t}) \Rightarrow P_t > f & \end{cases} \quad (3)$$

304 where C is a coefficient of soil saturation obtained by calibration, and $S_{w,\text{max}}$ is the content of
 305 water at saturation point which depends on the nature of the soil and on its use.

306 The sub-surface flow is considered proportional to the difference between the water content $S_{w,t}$
 307 at time t and that at soil capacity S_c :

$$308 \quad R_{\text{sub},t} = c \cdot (S_{w,t} - S_c) \quad (4)$$

309 while the estimated deep flow is evaluated according to the expression proposed by Laio et al.
 310 (2001):

$$311 \quad L_t = \frac{K_S}{e^{\beta \cdot \left(1 - \frac{S_c}{S_{w,\text{max}}} \right)} - 1} \cdot \left(e^{\beta \cdot \left(\frac{S_{w,t} - S_c}{S_{w,\text{max}}} \right)} - 1 \right) \quad (5)$$

312 where, K_S is the hydraulic conductivity of the soil in saturation conditions, β is a dimensionless
 313 exponent characteristic of the size and distribution of pores in the soil. The evaluation of the
 314 real evapotranspiration is performed assuming it as a function of the water content in the soil
 315 and potential evapotranspiration, calculated using the formulation of Hargreaves and Samani
 316 (1982).

317 Knowing the values of R_{sur} , R_{sub} and L , it is possible to model the surface Q_{sur} , sub-surface Q_{sub}
 318 and deep flow Q_g routed contributes according to the conceptual framework of the linear
 319 reservoir at the closing section of the single sub-catchment. In particular, in case of Q_{sur} the
 320 value of the parameter k , which is a function of the residence time in the catchment slopes, is
 321 estimated relating the velocity to the average slopes length. However, one of the challenges is
 322 to properly estimate such velocity, which should be calculated for each flood event (Rinaldo
 323 and Rodríguez-Iturbe, 1996). According to Rodríguez-Iturbe et al. (1982), this velocity is a

324 function of the effective rainfall intensity and the event duration. In this study, the estimation
325 of the surface velocity is performed using the relation between velocity and intensity of rainfall
326 excess proposed in Kumar et al. (2002), to then estimate the average travel time and the
327 consequent parameter k . However, this formulation is applied in a lumped way for a given sub-
328 catchment. As reported in McDonnell and Beven (2014), more reliable and distributed models
329 should be used to reproduce the spatial variability of the residence times over time within the
330 catchment. That is why, in the advanced version of the model implemented by AAWA, in each
331 sub-catchment the runoff propagation is carried out according to the geomorphological theory
332 of the hydrologic response. The overall catchment travel time distributions is considered as
333 nested convolutions of statistically independent travel time distributions along sequentially
334 connected, and objectively identified, smaller sub-catchments. The correct estimation of the
335 residence time should be derived considering the latest findings reported in McDonnell and
336 Beven (2014). Regarding Q_{sub} and Q_{g} , the value of k is calibrated comparing the observed and
337 simulated streamflow at Vicenza.

338 In the early warning system implemented by AAWA in the Bacchiglione catchment, the flood
339 propagation along the main river channel is represented by a one-dimensional hydrodynamic
340 model, MIKE 11 (DHI, 2005). However, in order to reduce the computational time required by
341 the analysis performed in this study, MIKE11 is replaced by a Muskingum-Cunge model (see,
342 e.g. Todini 2007), considering rectangular river cross-sections for the estimation of hydraulic
343 radii, wave celerities, and other hydraulic variables.

344 Calibration of the hydrological model parameters is performed by AAWA, and described in
345 Ferri et al. (2012), considering the time series of precipitation from 2000 to 2010 in order to
346 minimize the root mean square error between observed and simulated values of water level at
347 Ponte degli Angeli gauged station. In order to stay as close as possible to the early warning
348 system implemented by AAWA, we used the same calibrated model parameters proposed by
349 Ferri et al. (2012).

350 **3.2 Data assimilation procedure**

351 **3.2.1 Kalman Filter**

352 In data assimilation, it is typically assumed that the dynamic system can be represented in the
353 state-space as follows:

354
$$\mathbf{x}_t = M(\mathbf{x}_{t-1}, \mathcal{G}, I_t) + w_t \quad w_t \sim N(0, \mathbf{S}_t). \quad (6)$$

355
$$\mathbf{z}_t = H(\mathbf{x}_t, \mathcal{G}) + v_t \quad v_t \sim N(0, R_t). \quad (7)$$

356 where \mathbf{x}_t and \mathbf{x}_{t-1} are state vectors at time t and $t-1$, M is the model operator that propagates the
 357 states \mathbf{x} from its previous condition to the new one as a response to the inputs I_t , while H is the
 358 operator which maps the model states into output \mathbf{z}_t . The system and measurements errors w_t
 359 and v_t are assumed normally distributed with zero mean and covariance \mathbf{S} and R . In a
 360 hydrological modeling system, these states can represent the water stored in the soil (soil
 361 moisture, groundwater) or on the earth surface (snow pack). These states are one of the
 362 governing factors that determine the hydrograph response to the inputs into the catchment.

363 For the linear systems used in this study, the discrete state-space system of Eq. (1) can be
 364 represented as follows (Szilagyi and Szollosi-Nagy, 2010):

365
$$\mathbf{x}_t = \Phi \mathbf{x}_{t-1} + \Gamma I_t + w_t. \quad (8)$$

366
$$Q_t = \mathbf{H} \mathbf{x}_t + v_t. \quad (9)$$

367 where t is the time step, \mathbf{x} is the vector of the model states (stored water volume in m^3), Φ is the
 368 state-transition matrix (function of the model parameters n and k), Γ is the input-transition
 369 matrix and \mathbf{H} is the output matrix. For example, for $n=3$ the matrix \mathbf{H} is expressed as
 370 $\mathbf{H} = \begin{bmatrix} 0 & 0 & k \end{bmatrix}$. Expressions for matrices Φ and Γ can be found in Szilagyi and Szollosi-Nagy
 371 (2010).

372 For the Bacchiglione model (semi-distributed model), a preliminary sensitivity analysis on the
 373 model states (soil content S_w and the storage water x_{sur} , x_{sub} and x_L related to Q_{sur} , Q_{sub} and Q_g)
 374 is performed in order to decide on which of the states to update. The results of this analysis
 375 (shown in the next section) pointed out that the stored water volume x_{sur} (estimated using Eq.
 376 (8) with $n=1$, $H=k$ and I_t replaced by R_{sur}) is the most sensitive state and for this reason we
 377 decided to update only this state.

378 The Kalman Filter (KF, Kalman, 1960) is a mathematical tool which allows estimating, in an
 379 efficient computational (recursive) way, the state of a process which is governed by a linear
 380 stochastic difference equation. KF is optimal under the assumption that the error in the process
 381 is Gaussian; in this case, KF is derived by minimizing the variance of the system error assuming
 382 that the model state estimate is unbiased.

383 Kalman filter procedure can be divided into two steps, namely forecast equations, (Eqs. (10)
 384 and (11)), and update (or analysis) equations (Eqs. (12), (13) and (14)):

$$385 \quad \mathbf{x}_t^- = \Phi \mathbf{x}_{t-1}^+ + \Gamma \mathbf{I}_t. \quad (10)$$

$$386 \quad \mathbf{P}_t^- = \Phi \mathbf{P}_{t-1}^+ \Phi^T + \mathbf{S}. \quad (11)$$

$$387 \quad \mathbf{K}_t = \mathbf{P}_t^- \mathbf{H}^T (\mathbf{H} \mathbf{P}_t^- \mathbf{H}^T + R)^{-1}. \quad (12)$$

$$388 \quad \mathbf{x}_t^+ = \mathbf{x}_t^- + \mathbf{K}_t (Q_t^o - \mathbf{H} \mathbf{x}_t^-). \quad (13)$$

$$389 \quad \mathbf{P}_t^+ = (\mathbf{I} - \mathbf{K}_t \mathbf{H}) \mathbf{P}_t^-. \quad (14)$$

390 where \mathbf{K}_t is the Kalman gain matrix, \mathbf{P} is the error covariance matrix and Q^o is a new
 391 observation. In this study, the observed value of streamflow Q^o is equal to the synthetic CSD
 392 estimated as described above. The prior model states \mathbf{x} at time t are updated, as the response to
 393 the new available observation, using the analysis equations Eqs. (12) to (14). This allows for
 394 estimation of the values of the updated state (with superscript +) and then assessing the
 395 background estimates (with superscript -) for the next time step using the time update
 396 equations, Eqs. (10) and (11). The proper characterization of the model covariance matrix \mathbf{S} is
 397 a fundamental issue in Kalman filter. In this study, in order to evaluate the effect of assimilating
 398 CSD, small values of the model error \mathbf{S} are considered for each case study. In fact, a covariance
 399 matrix \mathbf{S} with diagonal values of $1 \text{ m}^6/\text{s}^2$, $25 \text{ m}^6/\text{s}^2$, and $1 \text{ m}^6/\text{s}^2$ are considered for the Brue,
 400 Sieve, and Alzette catchments. The bigger value of \mathbf{S} in the Sieve catchment is due to the higher
 401 flow magnitude in this catchment if compared to the other two. A sensitivity analysis of model
 402 performances depending on the value of \mathbf{S} is reported in the Results section. For the
 403 Bacchiglione catchment, \mathbf{S} is estimated, for each given flood event, as the variance between
 404 observed and simulated flow values.

405 3.2.2 Assimilation of crowdsourced data

406 As described in the previous section, a main characteristic of CSD is to be highly uncertain and
 407 asynchronous in time. Various methods have been proposed to include asynchronous
 408 observations in models. Having reviewed them, in this study we are proposing a somewhat
 409 simpler approach of Data Assimilation of Crowdsourced Observations (DACO). This method
 410 is based on the assumption that the change in the model states and in the error covariance

411 matrices within the two consecutive model time steps t_0 and t (observation window) is linear,
 412 while the inputs are assumed constant. All CSD received during the observation window are
 413 individually assimilated in order to update the model states and output at time t . Therefore,
 414 assuming that one CSD is available at time t_0^* , the first step of DACO (A in Figure 4) is the
 415 definition of the model states and error covariance matrix at t_0^* as:

$$416 \quad \mathbf{x}_{t_0}^- = \mathbf{x}_{t_0}^+ + (\mathbf{x}_t^- - \mathbf{x}_{t_0}^+) \cdot \frac{t_0^* - t_0}{t - t_0}. \quad (15)$$

$$417 \quad \mathbf{P}_{t_0}^- = \mathbf{P}_{t_0}^+ + (\mathbf{P}_t^- - \mathbf{P}_{t_0}^+) \cdot \frac{t_0^* - t_0}{t - t_0}. \quad (16)$$

418 The second step (B in Figure 4) is the estimation of the updated model states and error
 419 covariance matrix, as the response to the streamflow CSD $Q_{t_0}^o$. The estimation of the posterior
 420 values of $\mathbf{x}_{t_0}^-$ and $\mathbf{P}_{t_0}^-$ is performed by Eqs. (13) and (14) respectively. The Kalman gain is
 421 estimated by Eq. (12), where the prior values of model states and error covariance matrix at t_0^*
 422 are used. Knowing the posterior value $\mathbf{x}_{t_0}^+$ and $\mathbf{P}_{t_0}^+$ it is possible to predict the value of states
 423 and covariance matrix at one model step ahead, t^* (C in Figure 4) using the model forecast
 424 equations, Eqs. (10) and (11).

425 The last step (D in Figure 4) is the estimation of the interpolated value of \mathbf{x} and \mathbf{P} at time step
 426 t . This is performed by means of a linear interpolation between the current values of \mathbf{x} and \mathbf{P} at
 427 t_0^* and t^* :

$$428 \quad \tilde{\mathbf{x}}_t^- = \mathbf{x}_{t_0}^- + (\mathbf{x}_{t^*}^- - \mathbf{x}_{t_0}^-) \cdot \frac{t - t_0^*}{t^* - t_0^*}. \quad (17)$$

$$429 \quad \tilde{\mathbf{P}}_t^- = \mathbf{P}_{t_0}^- + (\mathbf{P}_{t^*}^- - \mathbf{P}_{t_0}^-) \cdot \frac{t - t_0^*}{t^* - t_0^*}. \quad (18)$$

430 The symbol \sim is added on the new matrices \mathbf{x} and \mathbf{P} in order to differentiate them from the
 431 original forecasted values in t . Assuming that a new streamflow CSD is available at an
 432 intermediate time t_1^* (between t_0^* and t), the procedure is repeated considering the values at t_0^*
 433 and t for the linear interpolation. Then, when no more CSD are available, the updated value of
 434 $\tilde{\mathbf{x}}_t^-$ is used to predict the model states and output at $t+1$ (Eqs. (10) and (11)). Finally, in order to
 435 account for the intermittent behavior of this CSD, the approach proposed by Mazzoleni et al.

436 (2015) is applied. In this method, the model states matrix \mathbf{x} is updated and forecasted when
437 CSD are available, while without CSD the model is run using Eq. (10) and covariance matrix
438 \mathbf{P} propagated at the next time step using Eq. (11).

439 **3.2.3 Crowdsourced data accuracy**

440 In this section, the uncertainty related to CSD is characterized. The observational error is
441 assumed normally distributed noise with zero mean and given standard deviation:

$$442 \quad \sigma_t^o = \alpha_t \cdot Q_t^o \quad (19)$$

443 where the coefficient α is related to the degree of uncertainty of the measurement (Weerts and
444 El Serafy, 2006).

445 One of the main and obvious issues in citizen-based observations is to maintain the quality
446 control of the water observations (Cortes et al., 2014; Engel and Voshell, 2002). In the
447 Introduction section, a number of methods to estimate the model of observational uncertainty
448 has been referred to. In this study, coefficient α is assumed a random variable uniformly
449 distributed between 0.1 and 0.3, so we leave more thorough investigation of uncertainty level
450 of CSD for future studies. We assumed that the maximum value of α is three times higher than
451 the uncertainty coming from the physical sensors due to the uncertain estimation of the rating
452 curve at the social sensor location.

453 **3.3 Experimental setup**

454 In this section, two sets of experiments are performed in order to test the proposed method and
455 assess the benefit of integrating CSD, asynchronous in time and with variable accuracies, in
456 real-time flood forecasting.

457 In the first set of experiments, called “Experiment 1”, assimilation of streamflow CSD at one
458 social sensor location is carried out in the Brue, Alzette, and Sieve catchments to understand
459 the sensitivity of the employed hydrological model - KMN - under various scenarios of these
460 data.

461 In the second set of experiments, called “Experiment 2”, the distributed CSD coming from
462 social and physical sensors, at four locations within the Bacchiglione catchment, are considered,
463 with the aim of assessing the improvement in the flood forecasting accuracy.

464 **3.3.1 Experiment 1: Assimilation of crowdsourced data from one social sensor**

465 The focus of Experiment 1 is to study the performance of the hydrological model (KMN)
466 assimilating CSD, having lower arrival frequencies than the model time step and random
467 accuracies, coming from a social sensor located at the outlet point of the Brue, Sieve and Alzette
468 catchments.

469 To analyse all possible combinations of arrival frequencies, number of CSD within the
470 observation window (1 hour) and accuracies, a set of scenarios are considered (Figure 5),
471 changing from regular arrival frequencies of CSD with high accuracies (scenario 1) to random
472 and chaotic asynchronous CSD with variable accuracies (scenario 11). In each scenario, a
473 varying number of CSD from 1 to 100 is considered. It is worth noting that for one CSD per
474 hour and regular arrival time, scenario 1 corresponds to the case of physical sensors with
475 observation arrival frequencies of one hour.

476 Scenario 2 corresponds to the case of CSD having fixed accuracies (α equal to 0.1) and irregular
477 arrival moments, but in which at least one CSD coincides with the model time step. In
478 particular, scenario 1 and 2 coincide for one CSD available within the observation window
479 since it is assumed that the arrival frequencies of that CSD have to coincide with the model
480 time step. On the other hand, the arrival frequencies of CSD in scenario 3 are assumed random
481 and CSD might not arrive at the model time step.

482 Scenario 4 considers CSD with regular frequencies but random accuracies at different moments
483 within the observation window, whereas in scenario 5 CSD have irregular arrival frequencies
484 and random accuracies. In all the previous scenarios the arrival frequencies, the number and
485 accuracies of CSD are assumed periodic, i.e. repeated between consecutive observation
486 windows along all the time series. However, this periodic repetitiveness might not occur in real-
487 life, and for this reason, a non-periodic behavior is assumed in scenarios 6, 7, 8 and 9. The non-
488 periodicity assumptions of the arrival frequencies and accuracies are the only factors that
489 differentiate scenarios 6, 7, 8 and 9 from the scenarios 2, 3, 4, and 5 respectively. In addition,
490 the non-periodicity of the number of CSD within the observation window is introduced in
491 scenario 10.

492 Finally, in scenario 11 CSD, in addition to all the previous characteristics, might have an
493 intermittent behavior, i.e. not being available for one or more observation windows.

494 **3.3.2 Experiment 2: Spatially distributed physical and social sensors**

495 Synthetic CSD with the characteristics reported in scenarios 10 and 11 of Experiment 1 are
496 generated due to the unavailability of streamflow CSD during this study. In order to evaluate
497 the model performances, observed and simulated streamflows are compared, for different lead
498 times.

499 Streamflow data from physical sensors are assimilated in the hydrological model of AMICO
500 system at an hourly frequency, while CSD from social sensors are assimilated using the DACO
501 method previously described. The updated hydrograph estimated by the hydrological model is
502 used as the input into Muskingum-Cunge model used to propagate the streamflow downstream,
503 to the gauged station at Ponte degli Angeli, Vicenza.

504 The main goal of Experiment 2 is to understand the contribution of distributed CSD to the
505 improvement of the flood prediction at a specific point of the catchment, in this case at Ponte
506 degli Angeli. For this reason, five different settings are introduced, and represented in Figure
507 6, corresponding to different types of employed sensors.

508 Firstly, only streamflow data from one physical sensor at the Leogra sub-catchment are
509 assimilated to update the hydrological model of sub-catchment B (Figure 2) of setting A (Figure
510 6). On the other hand, in setting B, CSD from the social sensor located at the Leogra sub-
511 catchment are assimilated. In setting C, CSD from three distributed social sensors are integrated
512 into the hydrological model. Setting D accounts for the integration of CSD from two social
513 sensors and physical data from the physical sensor in the Leogra sub-catchment. Finally, setting
514 E considers the complete integration between physical and social sensors in Leogra and the two
515 social sensors in the Timonchio and Orolo sub-catchments.

516 **4 Results**

517 **4.1 Experiment 1: Influence of crowdsourced data on flood forecasting**

518 The observed and simulated streamflow hydrographs at the outlet section of the Brue, Sieve
519 and Alzette catchments with and without the model update (considering hourly streamflow
520 data) are reported in Figure 7 for nine different flood events for 1-hour lead time. As expected,
521 it can be seen that the updated model tends to better represent the flood events than the model
522 without updating in all the case studies. However, this improvement it is closely related to the

523 value of the matrix \mathbf{S} . The higher the \mathbf{S} value (uncertain model) the closer the model output gets
524 to the observation. For this reason, a sensitivity analysis on the influence of the matrix \mathbf{S} on the
525 assimilation of CSD for scenario 1, i.e. coming and assimilated at regular time steps within the
526 observation windows, is reported in Figure 8. The results of Figure 8 are related to the first
527 flood event of the Brue, Sieve, and Alzette catchments. Increasing the number of CSD within
528 the observation window results in an improvement of the N_{SE} for different values of model
529 error. However, this improvement becomes negligible for a given threshold value of CSD,
530 which is a function of the considered flood event. This means that the additional CSD do not
531 add information useful for improving the model performance. Overall, increasing the value of
532 the model error \mathbf{S} tends to increase N_{SE} values as mentioned before. For this reason, to better
533 evaluate the effect of assimilating CSD, a small value of \mathbf{S} , i.e. model more accurate than CSD,
534 is assumed.

535 In case scenario 1, the arrival frequencies are set as regular for different model runs, so the
536 moments and accuracies in which CSD became available are always the same for any model
537 run. However, for the other scenarios, the irregular moments in which CSD becomes available
538 within the observation window and their accuracies are randomly selected and change
539 according to the different model runs. This reflects in a random model performances and
540 consequent N_{SE} values. In order to remove such random behavior, different model runs (100 in
541 this case) are carried out, assuming different random values of arrivals and accuracies
542 (coefficient α) during each model run, for a given number of CSD and lead time. The N_{SE} value
543 is estimated for each model run, so $\mu_{N_{SE}}$ and $\sigma_{N_{SE}}$ represent the mean and standard deviation
544 of the different values of N_{SE} .

545 For scenarios 2 and 3 (represented using warm, red and orange, colours in Figure 9 and Figure
546 10 for lead time equal to 24 h), the $\mu_{N_{SE}}$ values are smaller but comparable with the ones got
547 for scenario 1 for all the considered flood events and case studies. In particular, scenario 3 has
548 lower $\mu_{N_{SE}}$ than scenario 2. This can relate to the fact that both scenarios have random arrival
549 frequencies, however, in scenario 3 CSD are not provided at model time steps, as opposed to
550 scenario 2. From Figure 10, higher values of $\sigma_{N_{SE}}$ can be observed for scenario 3. Scenario 2
551 has the lowest standard deviation for low values of CSD because the arrival frequencies have
552 to coincide with the model time step and this stabilizes the N_{SE} . In particular, for an increasing
553 number of CSD $\sigma_{N_{SE}}$ tends to decrease. However, a constant trend of $\sigma_{N_{SE}}$ can be observed,

554 due to particular characteristics of the flood events, in case of the flood event 1 of Sieve and
555 flood event 2 and 3 of Alzette. It is worth nothing that scenario 1 has null standard deviation
556 because CSD are assumed coming at the same moments with the same accuracies for all 100
557 model runs.

558 In scenario 4, represented using blue color, CSD are considered coming at regular time steps
559 but having random accuracies. Figure 9 shows that $\mu_{N_{SE}}$ values are lower for scenario 4 than
560 for scenarios 2 and 3. This is related to the higher influence of CSD accuracies if compared to
561 arrival frequencies. High variability in the model performances, especially for low values of
562 CSD, it can be observed in scenario 4 (Figure 10).

563 The combined effects of random arrival frequencies and CSD accuracies is represented in
564 scenario 5 using a magenta color (i.e. the combination of warm and cold colors used for
565 scenarios 2, 3 and 4) in Figure 9 and Figure 10. As expected, this scenario has the lowest $\mu_{N_{SE}}$
566 and the highest $\sigma_{N_{SE}}$ values, compared to those reported above.

567 The remaining scenarios, from 6 to 9, are equivalent to the ones from 2 to 5 with the only
568 difference that they are non-periodic in time. For this reason, in Figure 9 and Figure 10,
569 scenarios from 6 to 9 have the same color of scenarios 2 to 5 but indicated with a dashed line
570 in order to underline their non-periodic behavior. Overall, it can be observed that non-periodic
571 scenarios have similar $\mu_{N_{SE}}$ values to their corresponding periodic scenario. However, the
572 smoother $\mu_{N_{SE}}$ trends can be explained because of the lower $\sigma_{N_{SE}}$ values, which means that
573 model performances are less dependent on the non-periodic nature of CSD than their period
574 behavior. Table 1 shows the N_{SE} values and model improvement obtained for the different
575 experimental scenarios during the different flood events. Small improvements are obtained
576 when N_{SE} is already high for 1 CSD as for the Sieve catchment during flood event 2 or the
577 Alzette catchment in the event 2. Moreover, it can be seen that a lower improvement is achieved
578 for scenarios (2, 3, 6 and 7) where arrival frequencies are random and accuracies fixed if
579 compared to those scenarios (4, 5, 8 and 9) where arrival frequencies are regular and accuracies
580 random.

581 In the previous analysis, model improvements are expressed only in terms of N_{SE} . However,
582 statistics such as N_{SE} only explain the overall model accuracy and not the real
583 increases/decreases in prediction error. Therefore, increases in model accuracy due to the

584 assimilation of CSD have to be presented in different ways as increased accuracy of flood peak
 585 magnitudes and timing. For this reason, additional analyses are carried out to assess the change
 586 in flood peak prediction considering three peaks occurred during flood event 2 in Brue
 587 catchment (see Figure 7). Errors in the flood peak timing, E_{RRT} , and intensity, E_{RRI} , are estimated
 588 as:

$$589 \quad E_{RRT} = t_p^o - t_p^s. \quad (20)$$

$$590 \quad E_{RRI} = \frac{Q_p^o - Q_p^s}{Q_p^o}. \quad (21)$$

591 where t_p^o and t_p^s are the observed and simulated peak time (h), while Q_p^o and Q_p^s are the
 592 observed and simulated peak streamflow (m^3/s). From the results reported in Figure 11,
 593 considering 12-h lead time, it can be observed that, overall, errors reduction in peak prediction
 594 is achieved for increasing number of CSD. In particular, assimilation of CSD has more
 595 influence in the reduction of the peak intensity rather than peak timing. In fact, a small reduction
 596 of E_{RRT} of about 1 h is obtained even increasing the number of CSD. In both E_{RRI} and E_{RRT} , the
 597 higher error reduction is obtained considering fixed CSD accuracies and random arrival
 598 frequencies (e.g. scenarios 1, 2, 3, 6 and 7). In fact, smaller E_{RRI} error values are obtained for
 599 scenario 1, while scenarios 5 and 9 are the ones that show the lowest improvement in terms of
 600 peak prediction. These conclusions are very similar to the previous ones obtained analyzing
 601 only N_{SE} as model performance measures.

602 The combination of all the previous scenarios is represented by scenario 10, where a changing
 603 number of CSD in each observation windows is considered. In scenario 11, the intermittent
 604 nature of CSD is accounted as well. The $\mu_{N_{SE}}$ and $\sigma_{N_{SE}}$ values of these scenarios obtained for
 605 the considered flood events are showed in Figure 12. It can be observed that scenarios 10 tends
 606 to provide higher $\mu_{N_{SE}}$ and lower $\sigma_{N_{SE}}$ values, for a given flood event, if compared to scenarios
 607 11. In fact, intermittency in CSD tends to reduce model performance and increase the variability
 608 of N_{SE} values for random configuration of arrival frequencies and CSD accuracies. In particular,
 609 $\sigma_{N_{SE}}$ tends to be constant for increasing number of CSD.

610 4.2 Experiment 2: Influence of distributed physical and social sensors

611 Three different flood events occurred in the Bacchiglione catchment are used for the
612 Experiment 2. Figure 13 shows the observed and simulated streamflow value at the outlet
613 section of Vicenza. In particular, two simulated time series of streamflow are calculated using
614 as input for the hydrological model the measured and forecasted time series of precipitation.
615 Overall, an underestimation of the observed streamflow can be observed using forecasted input
616 while the results achieved using measured precipitation tend to properly represent the
617 observations. In order to find out what model states lead to a maximum increase of the model
618 performance, a preliminary sensitivity analysis is performed. The four model states, x_S , x_{sur} , x_{sub}
619 and x_L , related to S_w , Q_{sur} , Q_{sub} and Q_g , are uniformly perturbed by $\pm 20\%$ around the true state
620 value for every time step up to the perturbation time (PT). No correlation between time steps is
621 considered. After PT, the model realizations are run without perturbation in order to assess the
622 effect on the system memory. No assimilation, and no states update, is performed at this step.
623 From the results reported in Figure 14, related to the flood event 1, it can be observed that the
624 model state x_{sur} is the most sensitive state if compared to the other ones. In addition, the
625 perturbations of all the states seem to affect the model output even after the PT (high system
626 memory). For this reason, in this experiment, only the model state x_{sur} is updated by means of
627 the DACO method.

628 Scenarios 10 and 11, described in the previous sections, are used to represent the irregular and
629 random behavior of CSD assimilated in the Bacchiglione catchment.

630 Figure 15 and Figure 16 show the results obtained from the experiment settings represented in
631 Figure 6 during three different flood events. Three different lead time values are considered.
632 Different model runs (100) are performed to account for the effect induced by the random
633 arrival frequencies and accuracies of CSD within the observation window as described above.
634 Figure 15 shows that the assimilation of streamflow from the physical sensor in the Leogra sub-
635 catchment (setting A) provides a better streamflow prediction at Ponte degli Angeli if compared
636 to the assimilation of a small number of CSD provided by a social sensor in the same location
637 (setting B). In particular, Figure 15 shows that, depending on the flood event, the same N_{SE}
638 values achieved with the assimilation of physical data (hourly frequency and high accuracy)
639 can be obtained by assimilating between 10 and 20 CSD per hour for 4 h lead time. This number
640 of CSD tends to increase for increasing values of lead times. In case of intermittent CSD (Figure
641 16) the overall reduction of N_{SE} is such that even with a high number of CSD (even higher than

642 50 per hour) the N_{SE} is always lower than the one obtained assimilating physical streamflow
643 data for any lead time.

644 For setting C, it can be observed for all three flood events that distributed social sensors in
645 Timonchio, Leogra and Orolo sub-catchments allow for obtaining higher model performances
646 than the one achieved with only one physical sensor (see Figure 15). However, for flood event
647 3 this is valid only for small lead time values. In fact, for 8 and 12 h lead time values, the
648 contribution of CSD tend to decrease in favor of physical data from the Leogra sub-catchment.
649 This effect is predominant for intermittent CSD, scenario 11. In this case, setting C has higher
650 $\mu_{N_{SE}}$ values than setting A only during flood event 1 and for lead time values equal to 4 and 8
651 h (see Figure 16).

652 It is interesting to note that for setting D, during flood event 1, the $\mu_{N_{SE}}$ is higher than setting
653 C for low number of CSD. However, with a higher number of CSD, setting C is the one
654 providing the best model improvement for low lead time values. In the case of intermittent
655 CSD, it can be noticed that the setting D provides always higher improvement than setting C.
656 For flood event 1, the best model improvement is achieved for setting E, i.e. fully integrating
657 physical sensor with distributed social sensors. On the other hand, during flood events 2 and 3,
658 setting D shows higher improvements than setting E. For intermittent CSD the difference
659 between setting D and E tends to reduce for all the flood events. Overall, settings D and E are
660 the ones providing the highest $\mu_{N_{SE}}$ in both scenarios 10 and 11. This demonstrates the
661 importance of integrating an existing network of physical sensors (setting A) with social sensors
662 to improve flood predictions.

663 Figure 17 shows the standard deviation of the N_{SE} , $\sigma_{N_{SE}}$, obtained for the different settings for
664 4 h lead time. Similar results are obtained for the three flood events. In case of setting A, $\sigma_{N_{SE}}$
665 is equal to zero since CSD are coming from the physical sensor at regular time steps. Higher
666 $\sigma_{N_{SE}}$ values are obtained for setting B, while including distributed CSD (setting C) tend to
667 decrease the value of $\sigma_{N_{SE}}$. It can be observed that $\sigma_{N_{SE}}$ decreases for high values of CSD. As
668 expected, the lowest values of $\sigma_{N_{SE}}$ are achieved including the physical sensor in the data
669 assimilation procedure (setting D and E). Similar considerations can be drawn for intermittent
670 CSD, where higher and more perturbed $\sigma_{N_{SE}}$ values are obtained.

671 5 Discussion

672 The assimilation of CSD is performed in four different case studies considering only one social
673 sensor location in the Brue, Sieve, and Alzette catchments, and distributed social and physical
674 sensors within the Bacchiglione catchment.

675 In the first three catchments, different characteristics of CSD are represented by means of 11
676 scenarios. Nine different flood events are used to assess the beneficial use in assimilating CSD
677 in the hydrological model to improve flood forecasting.

678 Overall, assimilation of CSD improves model performances in all the considered case studies.
679 In particular, there is a limit in the number of CSD for which satisfactory model improvements
680 can be achieved, and for which additional CSD become redundant. This asymptotic behavior,
681 when extra information is added, has also been observed using other metrics by Krstanovic and
682 Singh (1992), Ridolfi et al. (2014), Alfonso et al. (2013)), among others. From Figure 9 it can
683 be seen that, in all the considered catchments, increasing the number of model error induces an
684 increase of this asymptotic value with a consequent reduction of CSD needed to improve model
685 performances. For this reason, a small value of the model error is assumed in this study. In
686 addition, it is not possible to define a priori number of CSD needed to improve model because
687 of its different behavior for a given flood event in case of no update. In fact, as reported in Table
688 1 and Figure 8, flood events with high N_{SE} values even without update tends to achieve the
689 asymptotic values of N_{SE} for small number of CSD (e.g. flood event 1 in Brue and 2 in Sieve),
690 while more CSD are needed for flood events having low N_{SE} without update. However, for
691 these case studies and during these nine flood events, an indicative value of 10 CSD can be
692 considered to achieve a good model improvement.

693 Figure 9 and Figure 10 show the $\mu_{N_{SE}}$ and $\sigma_{N_{SE}}$ values for the scenarios 2 to 9. Figure 9
694 demonstrate that for irregular arrival frequencies and constant accuracies (e.g. scenarios 2, 3, 6
695 and 7) the N_{SE} is higher than for scenarios in which accuracies are variable and arrival
696 frequencies fixed (e.g. scenarios 4, 5, 8 and 9). These results point out that the model
697 performance is more sensitive to the accuracies of CSD than to the moments in time at which
698 the streamflow CSD become available. Overall, $\sigma_{N_{SE}}$ tends to decrease for high number of
699 CSD. The combined effects of irregular frequencies and uncertainties are reflected in scenario
700 5, which has lower mean and higher standard deviation of N_{SE} if compared to the first four
701 scenarios.

702 An interesting fact is that, passing from periodic to non-periodic scenarios, the standard
703 deviation $\sigma_{N_{SE}}$ is significantly reduced, while $\mu_{N_{SE}}$ remains the same but with a smoother trend.
704 A non-periodic behavior of CSD, common in real life, helps to reduce the fluctuation of the N_{SE}
705 generated by the random behavior of streamflow CSD. Finally, the results obtained for
706 scenarios 10 and 11 are showed in Figure 12. The assimilation of irregular number of CSD in
707 scenario 10, in each observation window, seems to provide the similar $\mu_{N_{SE}}$ than the ones
708 obtained with scenario 9. One of the main outcomes is that the intermittent nature of CSD
709 (scenario 11) induces a drastic reduction of the N_{SE} and an increase in its noise in both
710 considered flood events. All these previous results are consistent across the considered
711 catchments.

712 In the case of the Bacchiglione catchment, the data from physical and social sensors are
713 assimilated within a hydrological model to improve the poor flow prediction in Vicenza for the
714 three considered flood events. In fact, these predictions are affected by an underestimation of
715 the 3-days rainfall forecast used as input in flood forecasting practice in this area.

716 One of the main outcomes of these analyses is that the replacement of a physical sensor (setting
717 A) for a social sensor at only one location (settings B) does not improve the model performance
718 in terms of N_{SE} for a small number of CSD. Figure 15 and Figure 16 show that distributed
719 locations of social sensors (setting C) can provide higher values of N_{SE} than a single physical
720 sensor, even for a low number of CSD, in case of CSD having the characteristic of scenario 10.
721 For flood event 1, setting C provides better model improvement than setting D for low lead
722 time values and high number of CSD. This can be because the physical sensor at Leogra
723 provides constant improvement, for a given lead time, while the social sensor tends to achieve
724 better results with a higher number of CSD. This dominant effect of the social sensor, for high
725 number of CSD, tends to increase for the higher lead times. On the other hand, for intermittent
726 CSD (scenario 11) this effect decreases in particular for flood events 2 and 3.

727 Integrating physical and social sensors (setting D and E) induces the highest model
728 improvements for all the three flood events. For flood event 1, assimilation from setting E it
729 appears to provide better results than assimilation from setting D. Opposite results are obtained
730 for flood events 2 and 3. In fact, the high $\mu_{N_{SE}}$ values of setting D can be because flood events
731 2 and 3 are characterized by one main peak and similar shape while flood event 1 has two main

732 peaks. Assimilation of CSD from distributed social sensors tends to reduce the variability of
733 the N_{SE} coefficient in both scenarios 10 and 11.

734 **6 Conclusions**

735 This study assesses the potential use of crowdsourced data in hydrological modeling, which are
736 characterized by irregular availability and variable accuracy. We demonstrate that even data
737 with these characteristics can improve flood prediction if integrated into hydrological models.
738 This opens new opportunities in terms of exploiting data being collected in current citizen
739 science projects for the modeling exercise. Our results do not support the idea that social-
740 sensors should partially or totally replace the existing network of physical sensors; instead, that
741 these new data should be used to compensate the lack of traditional observations. In fact, in
742 case of a dense network of physical sensors, the additional information from social sensors
743 might not be necessary because of the high accuracy of the hydrological observations derived
744 by physical sensors

745 Four different case studies, the Brue (UK), Sieve (Italy), Alzette (Luxemburg) and Bacchiglione
746 (Italy) catchments are considered, and the two types of hydrological models are used. In the
747 Experiment 1 (Brue, Sieve and Alzette catchments) the sensitivity of the model results to the
748 assimilation of crowdsourced data, having different frequencies and accuracies, derived from a
749 hypothetical social sensor at the catchments outlet is assessed. On the other hand, in the
750 Experiment 2 (Bacchiglione catchment), the influence of the combined assimilation of
751 crowdsourced data, from a distributed network of social sensors, and existing streamflow data
752 from physical sensors is evaluated. Because crowdsourced streamflow data are not yet available
753 in all case studies, realistic synthetic data with various characteristics of arrival frequencies and
754 accuracies are introduced.

755 Overall, we demonstrated that results are very similar in terms of model behavior assimilating
756 asynchronous data in all case studies.

757 In Experiment 1, it is found that increasing the number of crowdsourced data within the
758 observation window increases the model performance even if these data have irregular arrival
759 frequencies and accuracies. Moreover, data accuracy affects the average value of N_{SE} more than
760 the moment in which these data are assimilated. The noise in the N_{SE} is reduced when the
761 assimilated data are considered having non-periodic behavior. In addition, the intermittent
762 nature of the data tends to drastically reduce the N_{SE} of the model for different values of lead

763 times. In fact, if the intervals between the data are too large then the abundance of crowdsourced
764 data at other times and places is no longer able to compensate their intermittency.

765 Experiment 2 showed that, in the Bacchiglione catchment, the integration of data from social
766 sensors and a single physical sensor could improve the flood prediction even for a small number
767 of intermittent crowdsourced data. In case of both physical and social sensors located at the
768 same place, the assimilation of physical data gives the same model improvement than the
769 assimilation of high number and non-intermittent behavior of crowdsourced data. Overall, the
770 integration of existing physical sensors with a new network of social sensors can improve the
771 model predictions. Although the cases and models are different, the presented study
772 demonstrated that the results obtained are very similar in terms of model behavior assimilating
773 asynchronous data.

774 Although we have obtained interesting results, this work has some limitations. Firstly, the
775 proposed method used to assimilate crowdsourced data is applied to the linear parts of
776 hydrological models. This means that the proposed methodology has to be tested on models
777 with non-linear dynamics. Secondly, while realistic synthetic streamflow data are used in this
778 study, the developed methodology is not tested with data coming from actual social sensors.
779 Therefore, the conclusions need to be confirmed using real crowdsourced observations of water
780 level. Finally, advancing methods for a more accurate assessment of the data quality and
781 accuracy of data derived from social sensors need to be considered (e.g. developing a pre-
782 filtering module aimed to select only data having good accuracy while discarding the one with
783 low accuracy).

784 Future work will be aimed to address the limitations formulated above, which will allow for a
785 better characterization of the crowdsourced data, making them a reliable data source for model-
786 based forecasting.

787 **Acknowledgements**

788 This research was partly funded in the framework of the EC FP7 Project WeSenseIt: Citizen
789 Observatory of Water, grant agreement No. 308429. Data used were supplied by the British
790 Atmospheric Data Centre from the NERC Hydrological Radar Experiment Dataset
791 <http://www.badc.rl.ac.uk/data/hyrex/> and by the Alto Adriatico Water Authority (Italy). The
792 Authors wish to thank the Editor and two anonymous reviewers for their insightful and useful
793 comments.

795 **References**

- 796 ABC: ABC's crowdsourced flood-mapping initiative, ABCs Crowdsourced Flood-Mapp.
797 Initiat. [online] Available from:
798 <http://www.abc.net.au/technology/articles/2011/01/13/3112261.htm> (Accessed 20 January
799 2016), 2011.
- 800 Alberoni, P., Collier, C. and Khabiti, R.: ACTIF Best practice paper - Understanding and
801 reducing uncertainty in flood forecasting, Proceeding Act. Conf., (1), 1–43, 2005.
- 802 Alfonso, L.: Use of hydroinformatics technologies for real time water quality management and
803 operation of distribution networks. Case study of Villavicencio, Colombia, M.Sc. Thesis,
804 UNESCO-IHE, Institute for Water Education, Delft, The Netherlands., 2006.
- 805 Alfonso, L., He, L., Lobbrecht, A. and Price, R.: Information theory applied to evaluate the
806 discharge monitoring network of the Magdalena River, J. Hydroinformatics, 15(1), 211,
807 doi:10.2166/hydro.2012.066, 2013.
- 808 Alfonso, L., Chacon, J. and Pena-Castellanos. G.: Allowing Citizens to Effortlessly Become
809 Rainfall Sensors, in 36th IAHR World Congress edited, The Hague, the Netherlands, 2015.
- 810 Arnold, C. P. and Dey, C. H.: Observing-Systems Simulation Experiments: Past, Present, and
811 Future, Bull. Am. Meteorol. Soc., 67(6), 687–695, doi:10.1175/1520-
812 0477(1986)067<0687:OSSEPP>2.0.CO;2, 1986.
- 813 Au, J., Bagchi, P., Chen, B., Martinez, R., Dudley, S. A. and Sorger, G. J.: Methodology for
814 public monitoring of total coliforms, Escherichia coli and toxicity in waterways by Canadian
815 high school students, J. Environ. Manage., 58(3), 213–230, doi:10.1006/jema.2000.0323,
816 2000.
- 817 Aubert, D., Loumagne, C. and Oudin, L.: Sequential assimilation of soil moisture and
818 streamflow data in a conceptual rainfall–runoff model, J. Hydrol., 280(1–4), 145–161,
819 doi:10.1016/S0022-1694(03)00229-4, 2003.
- 820 Bergström, S.: Principles and confidence in hydrological modelling, Hydrol. Res., 22(2), 123–
821 136, 1991.
- 822 Bird, T. J., Bates, A. E., Lefcheck, J. S., Hill, N. A., Thomson, R. J., Edgar, G. J., Stuart-Smith,
823 R. D., Wotherspoon, S., Krkosek, M., Stuart-Smith, J. F., Pecl, G. T., Barrett, N. and Frusher,
824 S.: Statistical solutions for error and bias in global citizen science datasets, Biol. Conserv.,
825 173, 144–154, doi:10.1016/j.biocon.2013.07.037, 2014.

826 Bordogna, G., Carrara, P., Criscuolo, L., Pepe, M. and Rampini, A.: A linguistic decision
827 making approach to assess the quality of volunteer geographic information for citizen
828 science, *Inf. Sci.*, 258, 312–327, doi:10.1016/j.ins.2013.07.013, 2014.

829 Buytaert, W., Zulkafli, Z., Grainger, S., Acosta, L., Alemie, T. C., Bastiaensen, J., De Bièvre,
830 B., Bhusal, J., Clark, J., Dewulf, A., Foggin, M., Hannah, D. M., Hergarten, C., Isaeva, A.,
831 Karpouzoglou, T., Pandeya, B., Paudel, D., Sharma, K., Steenhuis, T., Tilahun, S., Van
832 Hecken, G. and Zhumanova, M.: Citizen science in hydrology and water resources:
833 opportunities for knowledge generation, ecosystem service management, and sustainable
834 development, *Front. Earth Sci.*, 2(October), 1–21, doi:10.3389/feart.2014.00026, 2014.

835 Canizares, R., Heemink, A. W. and Vested, H. J.: Application of advanced data assimilation
836 methods for the initialisation of storm surge models, *J. Hydraul. Res.*, 36(4), 655–674,
837 doi:10.1080/00221689809498614, 1998.

838 Célleri, R., Buytaert, W., De Bièvre, B., Tobón, C., Crespo, P., Molina, J. and Feyen, J.:
839 Understanding the hydrology of tropical Andean ecosystems through an Andean Network
840 of Basins, [online] Available from: <http://dspace.ucuenca.edu.ec/handle/123456789/22089>
841 (Accessed 19 February 2016), 2009.

842 Cifelli, R., Doesken, N., Kennedy, P., Carey, L. D., Rutledge, S. A., Gimmestad, C. and Depue,
843 T.: The Community Collaborative Rain, Hail, and Snow Network: Informal Education for
844 Scientists and Citizens, *Bull. Am. Meteorol. Soc.*, 86(8), 1069–1077, 2005.

845 Clark, M. P., Rupp, D. E., Woods, R. A., Zheng, X., Ibbitt, R. P., Slater, A. G., Schmidt, J. and
846 Uddstrom, M. J.: Hydrological data assimilation with the ensemble Kalman filter: Use of
847 streamflow observations to update states in a distributed hydrological model, *Adv. Water*
848 *Resour.*, 31(10), 1309–1324, doi:10.1016/j.advwatres.2008.06.005, 2008.

849 Cortes Arevalo, V. J., Charrière, M., Bossi, G., Frigerio, S., Schenato, L., Bogaard, T.,
850 Bianchizza, C., Pasuto, A. and Sterlacchini, S.: Evaluating data quality collected by
851 volunteers for first-level inspection of hydraulic structures in mountain catchments, *Nat.*
852 *Hazards Earth Syst. Sci.*, 14(10), 2681–2698, doi:10.5194/nhess-14-2681-2014, 2014.

853 Degrossi, L. C., Do Amaral, G. G., da Vasconcelos, E. S. M., Albuquerque, J. P. and Ueyama,
854 J.: Using Wireless Sensor Networks in the Sensor Web for Flood Monitoring in Brazil, in
855 *Proceedings of the 10th International ISCRAM Conference, Baden-Baden, Germany.*
856 [online] Available from:
857 [http://humanitariancomp.referata.com/wiki/Using_Wireless_Sensor_Networks_in_the_Sen](http://humanitariancomp.referata.com/wiki/Using_Wireless_Sensor_Networks_in_the_Sensor_Web_for_Flood_Monitoring_in_Brazil)
858 [sor_Web_for_Flood_Monitoring_in_Brazil](http://humanitariancomp.referata.com/wiki/Using_Wireless_Sensor_Networks_in_the_Sensor_Web_for_Flood_Monitoring_in_Brazil) (Accessed 10 February 2016), 2013.

859 Derber, J. and Rosati, A.: A Global Oceanic Data Assimilation System, *J. Phys. Oceanogr.*,
860 19(9), 1333–1347, doi:10.1175/1520-0485(1989)019<1333:AGODAS>2.0.CO;2, 1989.

861 DHI: MIKE FLOOD User Manual, 2005.

862 Drecourt, J.-P.: Data assimilation in hydrological modelling, Environment & Resources DTU.
863 Technical University of Denmark., 2004.

864 Eckhardt, K.: How to construct recursive digital filters for baseflow separation, *Hydrol.*
865 *Process.*, 19(2), 507–515, doi:10.1002/hyp.5675, 2005.

866 Engel, S. R. and Voshell Jr, J. R.: Volunteer biological monitoring: can it accurately assess the
867 ecological condition of streams?, *Am. Entomol.*, 48(3), 164–177, 2002.

868 Errico, R. M. and Privé, N. C.: An estimate of some analysis-error statistics using the Global
869 Modeling and Assimilation Office observing-system simulation framework, *Q. J. R.*
870 *Meteorol. Soc.*, 140(680), 1005–1012, doi:10.1002/qj.2180, 2014.

871 Errico, R. M., Yang, R., Privé, N. C., Tai, K.-S., Todling, R., Sienkiewicz, M. E. and Guo, J.:
872 Development and validation of observing-system simulation experiments at NASA’s Global
873 Modeling and Assimilation Office, *Q. J. R. Meteorol. Soc.*, 139(674), 1162–1178,
874 doi:10.1002/qj.2027, 2013.

875 Evensen, G.: Data Assimilation: The Ensemble Kalman Filter, 2nd ed. 2009 edition., Springer,
876 Place of publication not identified., 2006.

877 Fenicia, F., Solomatine, D. P., Savenije, H. H. G. and Matgen, P.: Soft combination of local
878 models in a multi-objective framework, *Hydrol. Earth Syst. Sci. Discuss.*, 4, 91–123,
879 doi:10.5194/hessd-4-91-2007, 2007.

880 Ferri, M., Monego, M., Norbiato, D., Baruffi, F., Toffolon, C. and Casarin, R.: La piattaforma
881 previsionale per i bacini idrografici del Nord Est Adriatico (I), in Proc.XXXIII Conference
882 of Hydraulics and Hydraulic Engineering, p. 10, Brescia., 2012.

883 Giandotti, M.: Previsione delle piene e delle magre dei corsi d’acqua, Servizio Idrografico
884 Italiano, Rome., 1933.

885 Hargreaves, G.H. and Samani, Z.A.: Estimating potential evapotranspiration, *J. Irrig. Drain.*
886 *Div.*, 108(3), 225–230, 1982.

887 Huang, B., Kinter, J. L. and Schopf, P. S.: Ocean data assimilation using intermittent analyses
888 and continuous model error correction, *Adv. Atmospheric Sci.*, 19(6), 965–992,
889 doi:10.1007/s00376-002-0059-z, 2002.

890 Hunt, B. R., Kalnay, E., Kostelich, E. J., Ott, E., Patil, D. J., Sauer, T., Szunyogh, I., Yorke, J.
891 A. and Zimin, A. V.: Four-dimensional Ensemble Kalman Filtering, *Tellus A*, 56(4), 273–
892 277, doi:10.1111/j.1600-0870.2004.00066.x, 2004.

893 Huwald, H., Barrenetxea, G., de Jong, S., Ferri, M., Carvalho, R., Lanfranchi, V., McCarthy,
894 S., Glorioso, G., Prior, S., Solà, E., Gil-Roldàn, E., Alfonso, L., Wehn de Montalvo, U.,
895 Onencan, A., Solomatine, D. and Lobbrecht, A.: D1.11 Sensor technology requirement
896 analysis, Confidential Deliverable, The WeSenseIt Project (FP7/2007-2013 grant agreement
897 no 308429)., 2013.

898 Ide, K., Courtier, P., Ghil, M. and Lorenc, A. C.: Unified notation for data assimilation:
899 operational, sequential and variational, *J. Meteorol. Soc. Jpn.*, 75(1B), 181–189, 1997.

900 ISPUW: iSPUW: Integrated Sensing and Prediction of Urban Water for Sustainable Cities,
901 [online] Available from: <http://ispuw.uta.edu/nsf/> (Accessed 19 February 2016), 2015.

902 Kalman, R. E.: A new approach to linear filtering and prediction problems, *J. Basic Eng.*, 82(1),
903 35–45, doi:10.1115/1.3662552, 1960.

904 Krstanovic, P. F. and Singh, V. P.: Evaluation of rainfall networks using entropy: II.
905 Application, *Water Resour. Manag.*, 6(4), 295–314, doi:10.1007/BF00872282, 1992.

906 Kumar, R., Chatterjee, C., Lohani, A. K., Kumar, S. and Singh, R. D.: Sensitivity Analysis of
907 the GIUH based Clark Model for a Catchment, *Water Resour. Manag.*, 16(4), 263–278,
908 doi:10.1023/A:1021920717410, 2002.

909 Laio, F., Porporato, A., Ridolfi, L. and Rodriguez-Iturbe, I.: Plants in water-controlled
910 ecosystems: active role in hydrologic processes and response to water stress: II. Probabilistic
911 soil moisture dynamics, *Adv. Water Resour.*, 24(7), 707–723, doi:10.1016/S0309-
912 1708(01)00005-7, 2001.

913 Li, Z. and Navon, I. M.: Optimality of variational data assimilation and its relationship with the
914 Kalman filter and smoother, *Q. J. R. Meteorol. Soc.*, 127(572), 661–683,
915 doi:10.1002/qj.49712757220, 2001.

916 Lowry, C. S. and Fienen, M. N.: CrowdHydrology: Crowdsourcing hydrologic data and
917 engaging citizen scientists, *GroundWater*, 51(1), 151–156, doi:10.1111/j.1745-
918 6584.2012.00956.x, 2013.

919 Macpherson, B.: Dynamic initialization by repeated insertion of data, *Q. J. R. Meteorol. Soc.*,
920 117(501), 965–991, doi:10.1002/qj.49711750105, 1991.

921 Madsen, H. and Cañizares, R.: Comparison of extended and ensemble Kalman filters for data
922 assimilation in coastal area modelling, *Int. J. Numer. Methods Fluids*, 31(6), 961–981,
923 doi:10.1002/(SICI)1097-0363(19991130)31:6<961::AID-FLD907>3.0.CO;2-0, 1999.

924 Massart, S., Pajot, B., Piacentini, A. and Pannekoucke, O.: On the merits of using a 3D-FGAT
925 assimilation scheme with an outer loop for atmospheric situations governed by transport,
926 *Mon. Weather Rev.*, 138(12), 4509–4522, 2010.

927 Matheron, G.: Principles of geostatistics, *Econ. Geol.*, 58(8), 1246–1266, 1963.

928 Mazzoleni, M., Alfonso, L. and Solomatine, D.: Influence of spatial distribution of sensors and
929 observation accuracy on the assimilation of distributed streamflow data in hydrological
930 modelling, *Hydrological Science Journal*, doi: 10.1080/02626667.2016.1247211, 2016.

931 Mazzoleni, M., Alfonso, L., Chacon-Hurtado, J. and Solomatine, D.: Assimilating uncertain,
932 dynamic and intermittent streamflow observations in hydrological models, *Adv. Water
933 Resour.*, 83, 323–339, 2015.

934 McDonnell, J. J. and Beven, K.: Debates—The future of hydrological sciences: A (common)
935 path forward? A call to action aimed at understanding velocities, celerities and residence
936 time distributions of the headwater hydrograph, *Water Resour. Res.*, 50(6), 5342–5350,
937 doi:10.1002/2013WR015141, 2014.

938 Moore, R. J., Jones, D. A., Cox, D. R. and Isham, V. S.: Design of the HYREX raingauge
939 network, *Hydrol. Earth Syst. Sci.*, 4(4), 521–530, doi:10.5194/hess-4-521-2000, 2000.

940 Ragnoli, E., Zhuk, S., Donncha, F. O., Suits, F. and Hartnett, M.: An optimal interpolation
941 scheme for assimilation of HF radar current data into a numerical ocean model, in *Oceans*,
942 2012, pp. 1–5., 2012.

943 Rakovec, O., Weerts, A. H., Hazenberg, P., F. Torfs, P. J. J. and Uijlenhoet, R.: State updating
944 of a distributed hydrological model with ensemble kalman Filtering: Effects of updating
945 frequency and observation network density on forecast accuracy, *Hydrol. Earth Syst. Sci.*,
946 16(9), 3435–3449, doi:10.5194/hess-16-3435-2012, 2012.

947 Rakovec, O., Weerts, A. H., Sumihar, J. and Uijlenhoet, R.: Operational aspects of
948 asynchronous filtering for flood forecasting, *Hydrol. Earth Syst. Sci.*, 19(6), 2911–2924,
949 doi:10.5194/hess-19-2911-2015, 2015.

950 Refsgaard, J. C.: Validation and Intercomparison of Different Updating Procedures for Real-
951 Time Forecasting, *Nord. Hydrol.*, 28(2), 65–84, doi:10.2166/nh.1997.005, 1997.

952 Ridolfi, E., Alfonso, L., Baldassarre, G. D., Dottori, F., Russo, F. and Napolitano, F.: An
953 entropy approach for the optimization of cross-section spacing for river modelling, *Hydrol.*
954 *Sci. J.*, 59(1), 126–137, doi:10.1080/02626667.2013.822640, 2014.

955 Rinaldo, A. and Rodriguez-Iturbe, I.: *Geomorphological Theory of the Hydrological Response*,
956 *Hydrol. Process.*, 10(6), 803–829, doi:10.1002/(SICI)1099-1085(199606)10:6<803::AID-
957 HYP373>3.0.CO;2-N, 1996.

958 Rodríguez-Iturbe, I., González-Sanabria, M. and Bras, R. L.: A geomorphoclimatic theory of
959 the instantaneous unit hydrograph, *Water Resour. Res.*, 18(4), 877–886,
960 doi:10.1029/WR018i004p00877, 1982.

961 Roy, H. E., Pocock, M. J. O., Preston, C. D., Roy, D. B. and Savage, J.: *Understanding Citizen*
962 *Science and Environmental Monitoring, Final Report of UK Environmental Observation*
963 *Framework.*, 2012.

964 Sakov, P., Evensen, G. and Bertino, L.: Asynchronous data assimilation with the EnKF, *Tellus*
965 *A*, 62(1), 24–29, doi:10.1111/j.1600-0870.2009.00417.x, 2010.

966 Seo, D. ., Kerke, B., Zink, M., Fang, N., Gao, J. and Yu, X.: *iSPUW: A Vision for Integrated*
967 *Sensing and Prediction of Urban Water for Sustainable Cities.*, 2014.

968 Solomatine, D. P. and Dulal, K. N.: Model trees as an alternative to neural networks in
969 rainfall—runoff modelling, *Hydrol. Sci. J.*, 48(3), 399–411,
970 doi:10.1623/hysj.48.3.399.45291, 2003.

971 Szilagyi, J. and Szollosi-Nagy, A.: *Recursive Streamflow Forecasting: A State Space Approach*
972 *- CRC Press Book.*, 2010.

973 Todini, E.: A mass conservative and water storage consistent variable parameter Muskingum-
974 Cunge approach, *Hydrol. Earth Syst. Sci.*, 11, 1645–1659, 2007.

975 Tulloch, A. I. T. and Szabo, J. K.: A behavioural ecology approach to understand volunteer
976 surveying for citizen science datasets, *Emu*, 112(4), 313, doi:10.1071/MU12009, 2012.

977 Vandecasteele, A. and Devillers, R.: Improving volunteered geographic data quality using
978 semantic similarity measurements, *ISPRS-Int. Arch. Photogramm. Remote Sens. Spat. Inf.*
979 *Sci.*, 1(1), 143–148, 2013.

980 Verlaan, M.: *Efficient Kalman Filtering Algorithms for Hydrodynamic Models*, PhD Thesis,
981 Delft University of Technology, The Netherlands., 1998.

982 Weerts, A. H. and El Serafy, G. Y. H.: Particle filtering and ensemble Kalman filtering for state
983 updating with hydrological conceptual rainfall-runoff models, *Water Resour. Res.*, 42(9), 1–
984 17, doi:10.1029/2005WR004093, 2006.

985 Wehn, U., Rusca, M., Evers, J. and Lanfranchi, V.: Participation in flood risk management and
986 the potential of citizen observatories: A governance analysis, *Environmental Science &*
987 *Policy*, 48, 225-236, 2015

988 WMO: Simulated real-time intercomparison of hydrological models, World Meteorological
989 Organization., 1992.

990 Wood, S. J., Jones, D. A. and Moore, R. J.: Accuracy of rainfall measurement for scales of
991 hydrological interest, *Hydrol. Earth Syst. Sci. Discuss.*, 4(4), 531–543, 2000

992

993

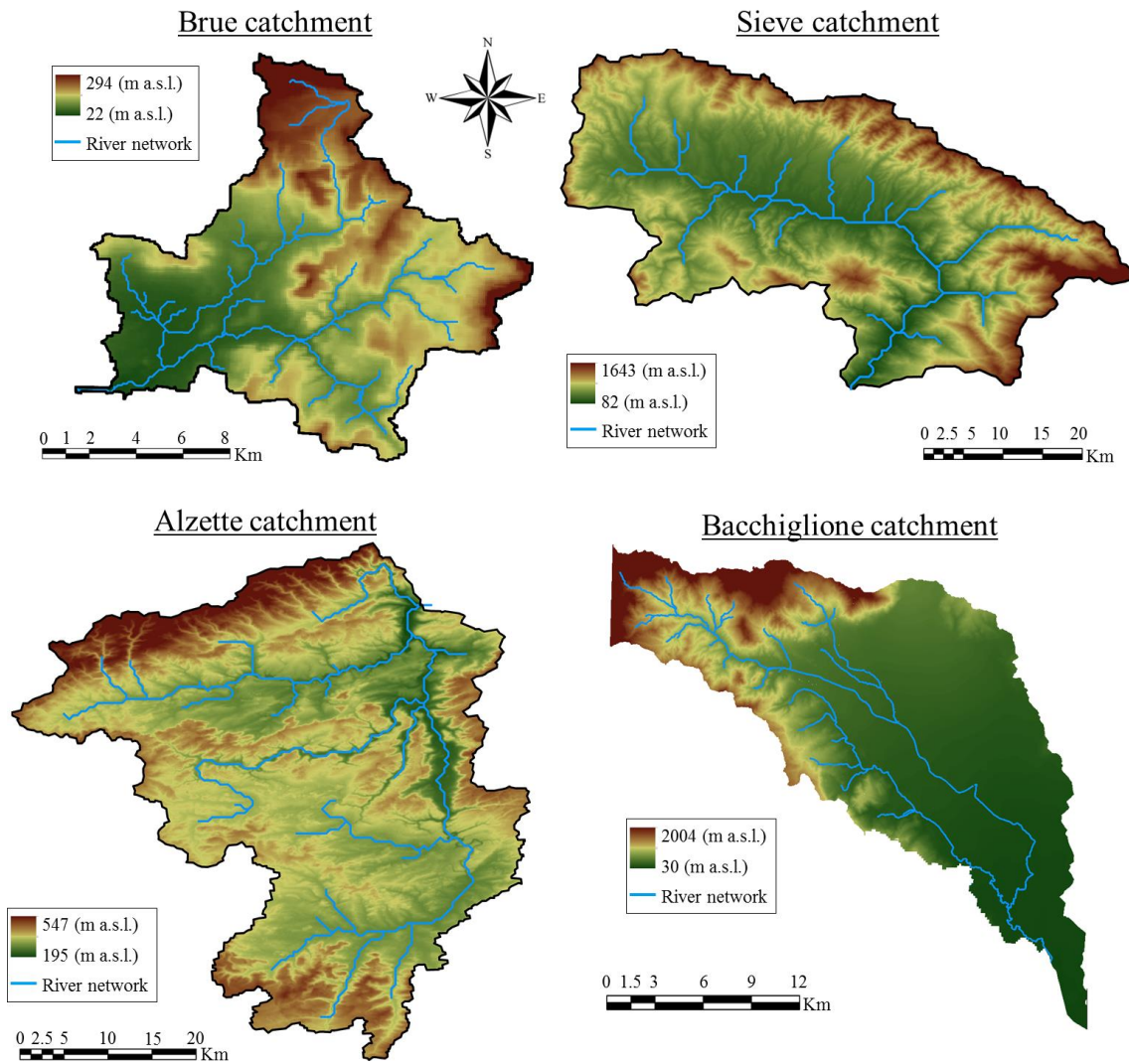
994 **Tables**

995

996 Table 1. N_{SE} improvements (%), from 1 to 50 CSD, for different experimental scenarios during
 997 the nine flood events occurred in the Brue, Sieve and Alzette catchments.

Scenario	1	2	3	4	5	6	7	8	9
Brue - event 1	0.126	0.125	0.140	0.243	0.253	0.125	0.144	0.237	0.248
Brue - event 2	0.416	0.413	0.445	0.920	0.902	0.413	0.463	0.841	0.870
Brue - event 3	0.443	0.438	0.472	0.890	0.842	0.440	0.471	0.809	0.822
Sieve - event 1	0.250	0.246	0.228	0.271	0.221	0.247	0.225	0.263	0.237
Sieve - event 2	0.066	0.064	0.067	0.057	0.056	0.064	0.068	0.057	0.060
Sieve - event 3	0.629	0.623	0.632	1.085	1.045	0.625	0.634	1.019	0.995
Alzette - event 1	0.884	0.881	0.883	1.274	1.265	0.882	0.890	1.251	1.342
Alzette - event 2	0.137	0.135	0.135	0.120	0.121	0.134	0.147	0.119	0.135
Alzette - event 3	0.314	0.309	0.305	0.297	0.283	0.310	0.315	0.297	0.281

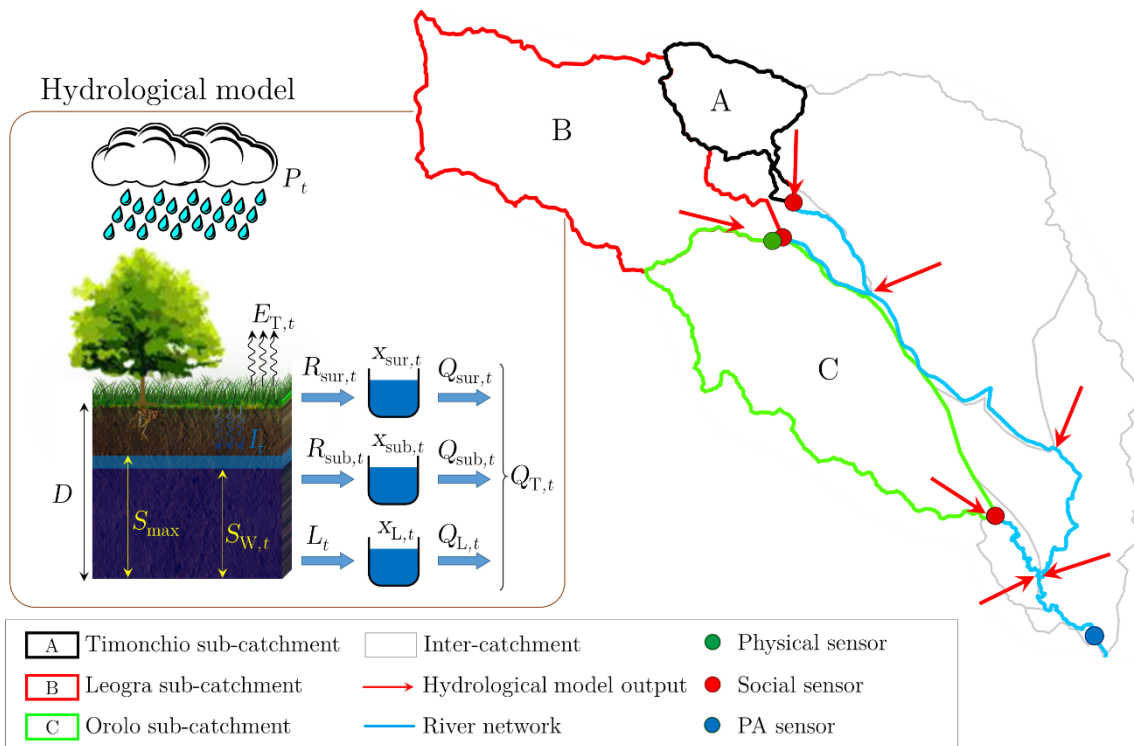
998



1000

1001 Figure 1. Representation of the four case studies considered in this study, clockwise: Brue
1002 catchment; Sieve catchment; Alzette catchment; Bacchiglione catchment.

1003



1004

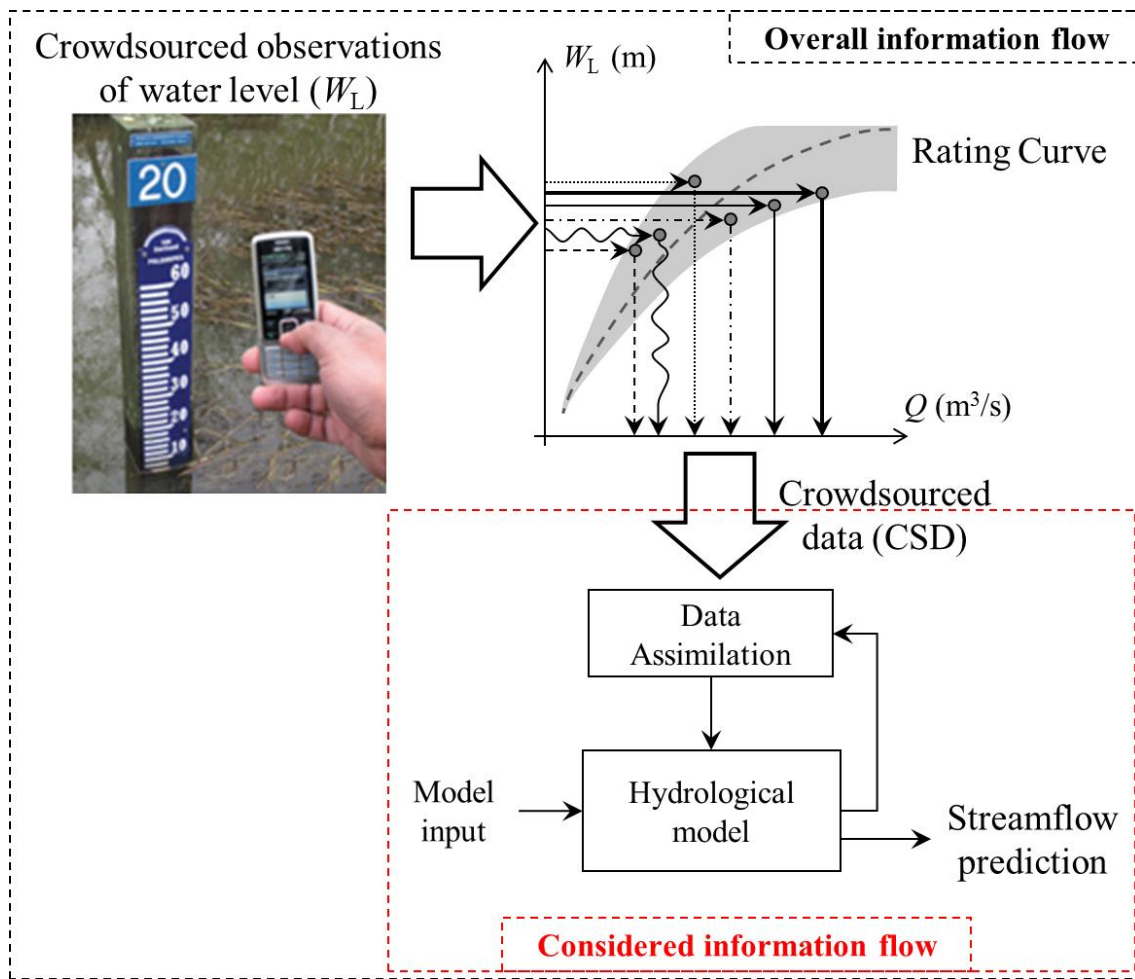
1005

1006

1007

1008

Figure 2. Structure of the hydrological model and location of the physical (green dots), social (red dots) and Ponte degli Angeli (PA, blue dots) sensors implemented in the Bacchiglione catchment by the Alto Adriatico Water Authority.



1009

1010

1011

1012

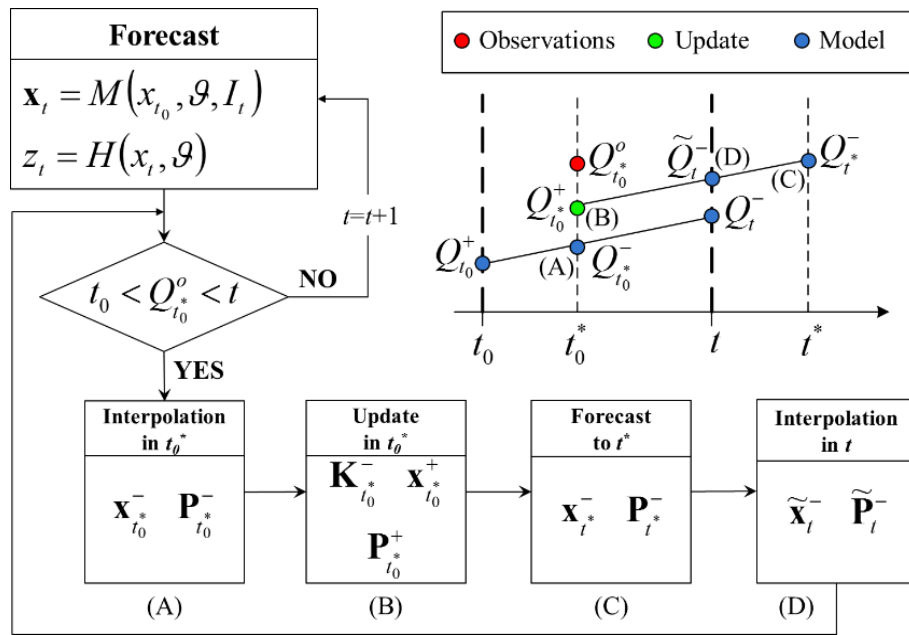
1013

1014

1015

1016

Figure 3. Graphical representation of the methodology proposed to estimate streamflow from crowdsourced observations of water level: a) crowdsourced observations of water level are turned into streamflow crowdsourced data (CSD), by means of rating curves assessed for the specific river location; b) assimilation of the streamflow crowdsourced data within the hydrological model.

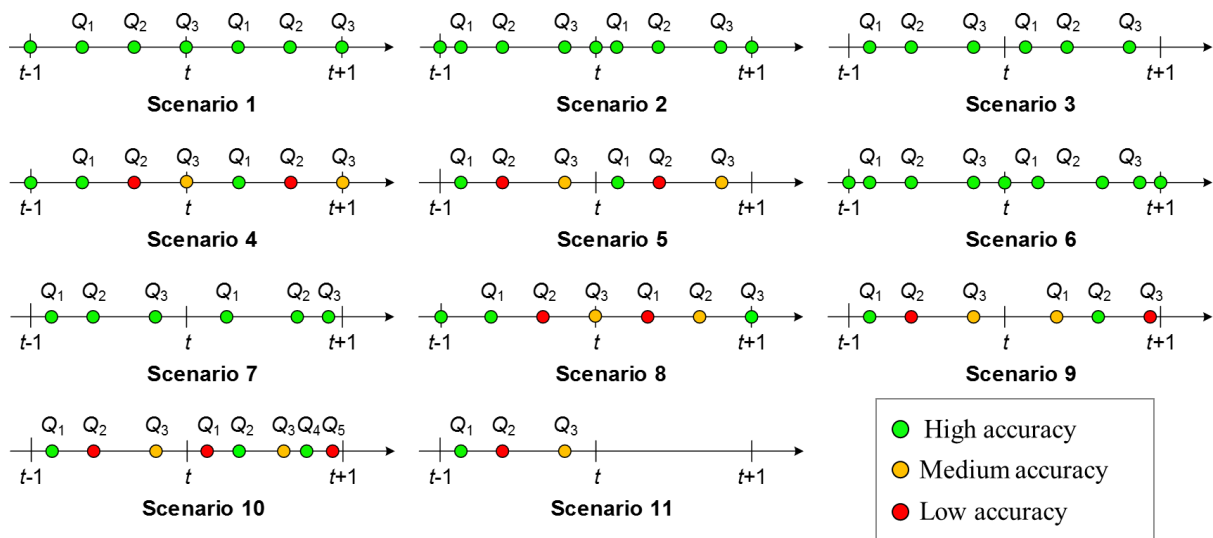


1017

1018 Figure 4. Graphical representation of the *data assimilation of crowdsourced observations*

1019 (DACO) method used in this study to assimilate asynchronous streamflow crowdsourced data.

1020

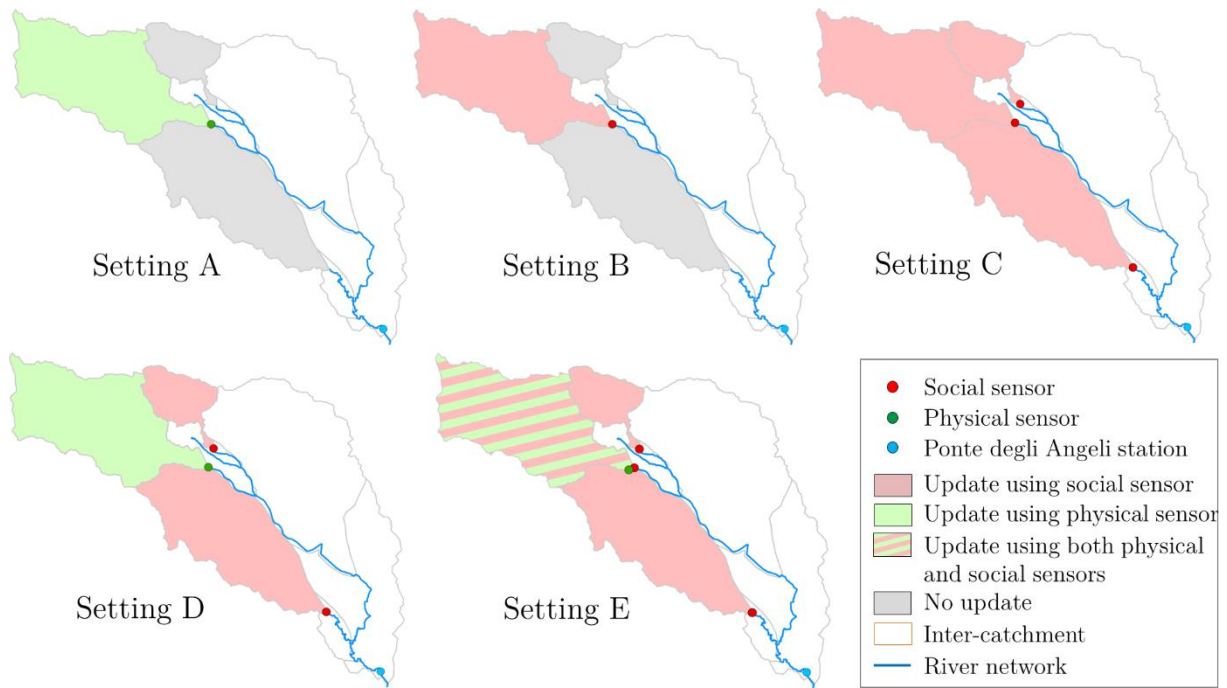


1021

1022 Figure 5. Experimental scenarios representing different configurations of arrival frequencies,

1023 number and accuracies of streamflow crowdsourced data.

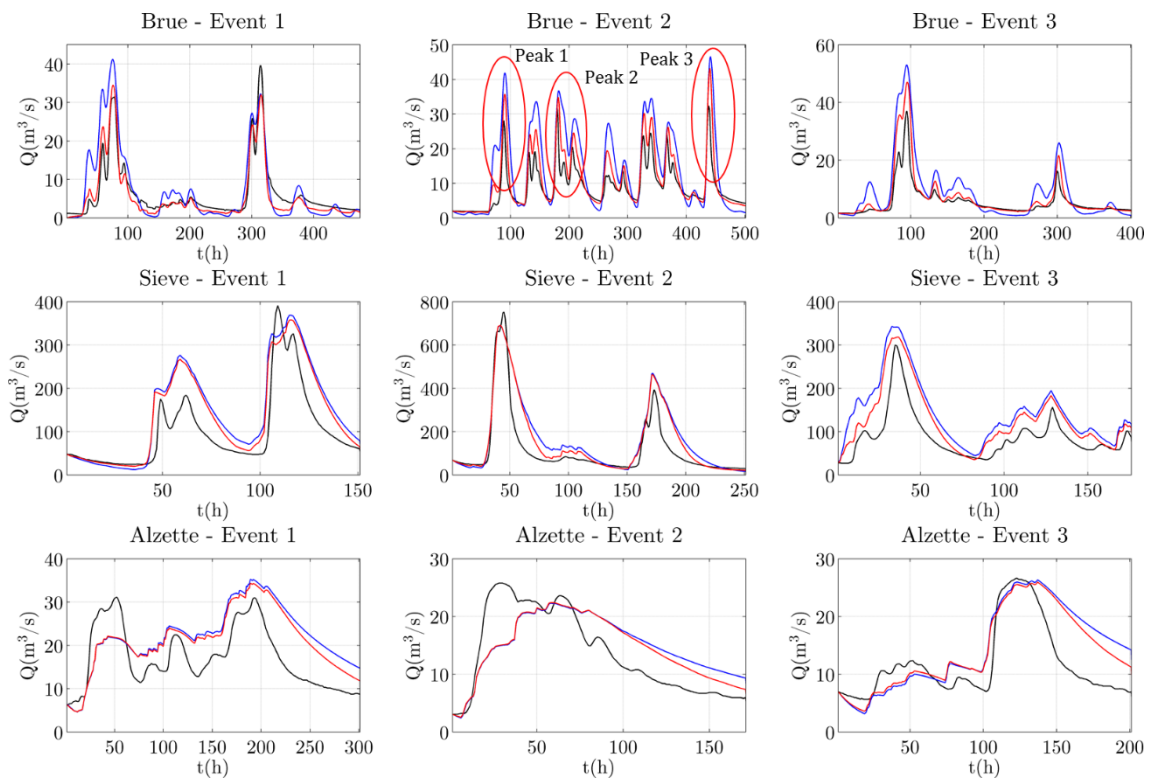
1024



1025

1026 Figure 6. Experiment 2: characteristics of the 5 experimental settings (A to E) implemented
 1027 within the Bacchiglione catchment: location of the social and physical sensors (dots),
 1028 hydrological model update based on different sensors (coloured areas).

1029



1030

1031 Figure 7. Observed (black line) and simulated hydrographs, with (red line) and without (blue

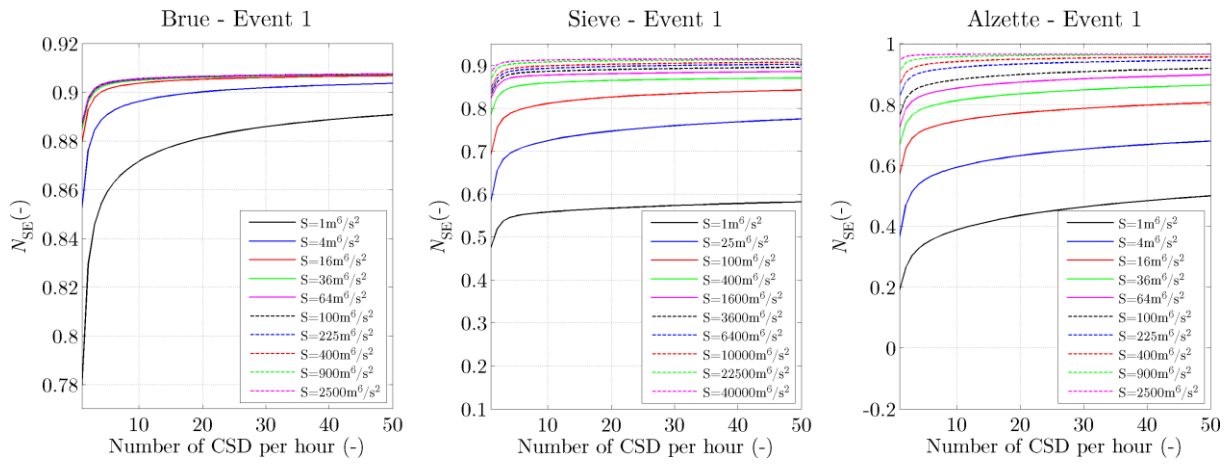
1032

1032 line) assimilation, for the flood events occurred in the three catchments: Brue (upper row), Sieve

1033

1033 (middle row) and Alzette (bottom row).

1034



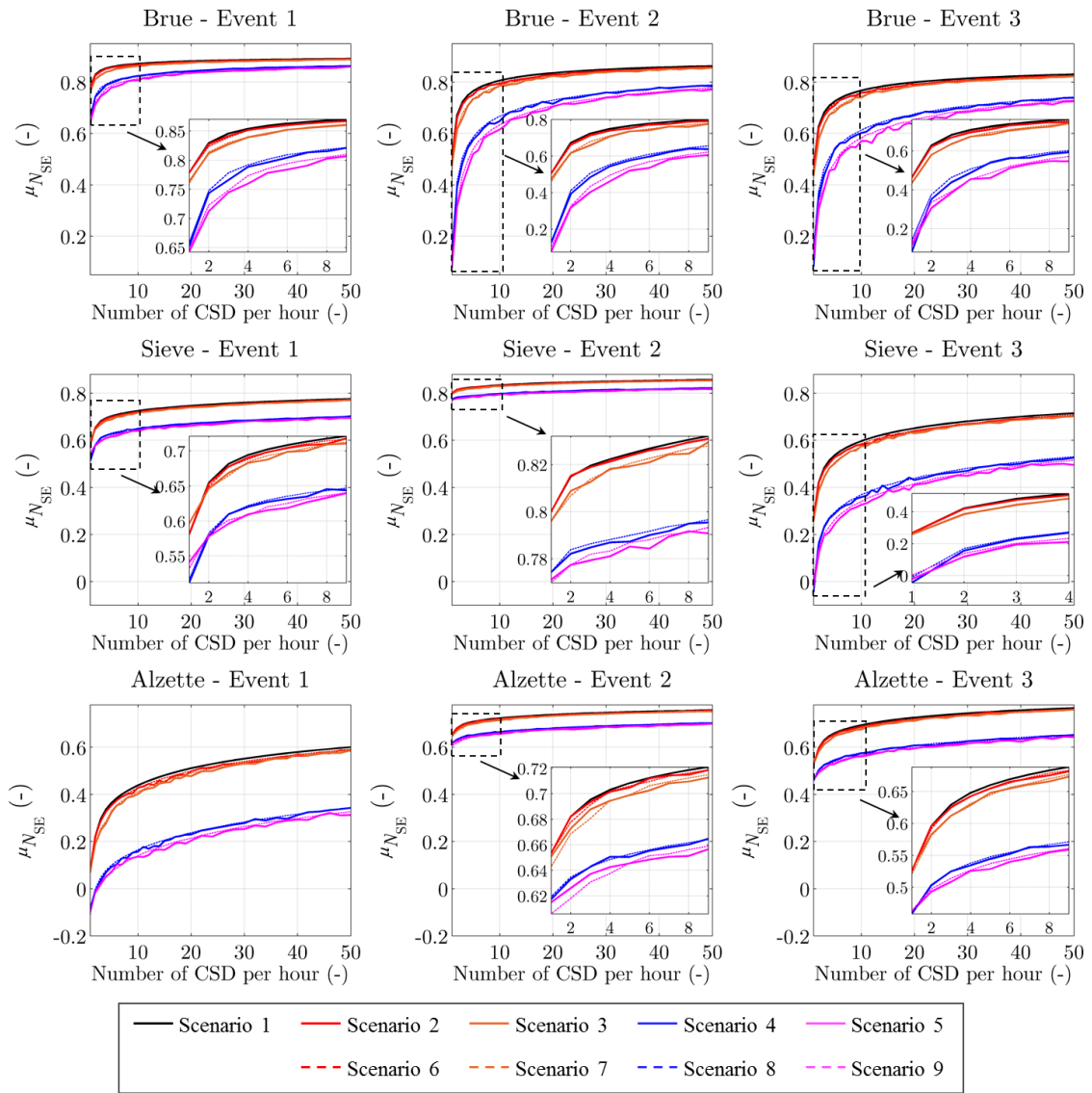
1035

1036

Figure 8. Model improvement in terms of Nash-Sutcliffe efficiency (N_{SE}) during flood event 1 for each case study, for different values of the model error matrix S and 24-h lead time, assimilating streamflow CSD according to scenario 1.

1039

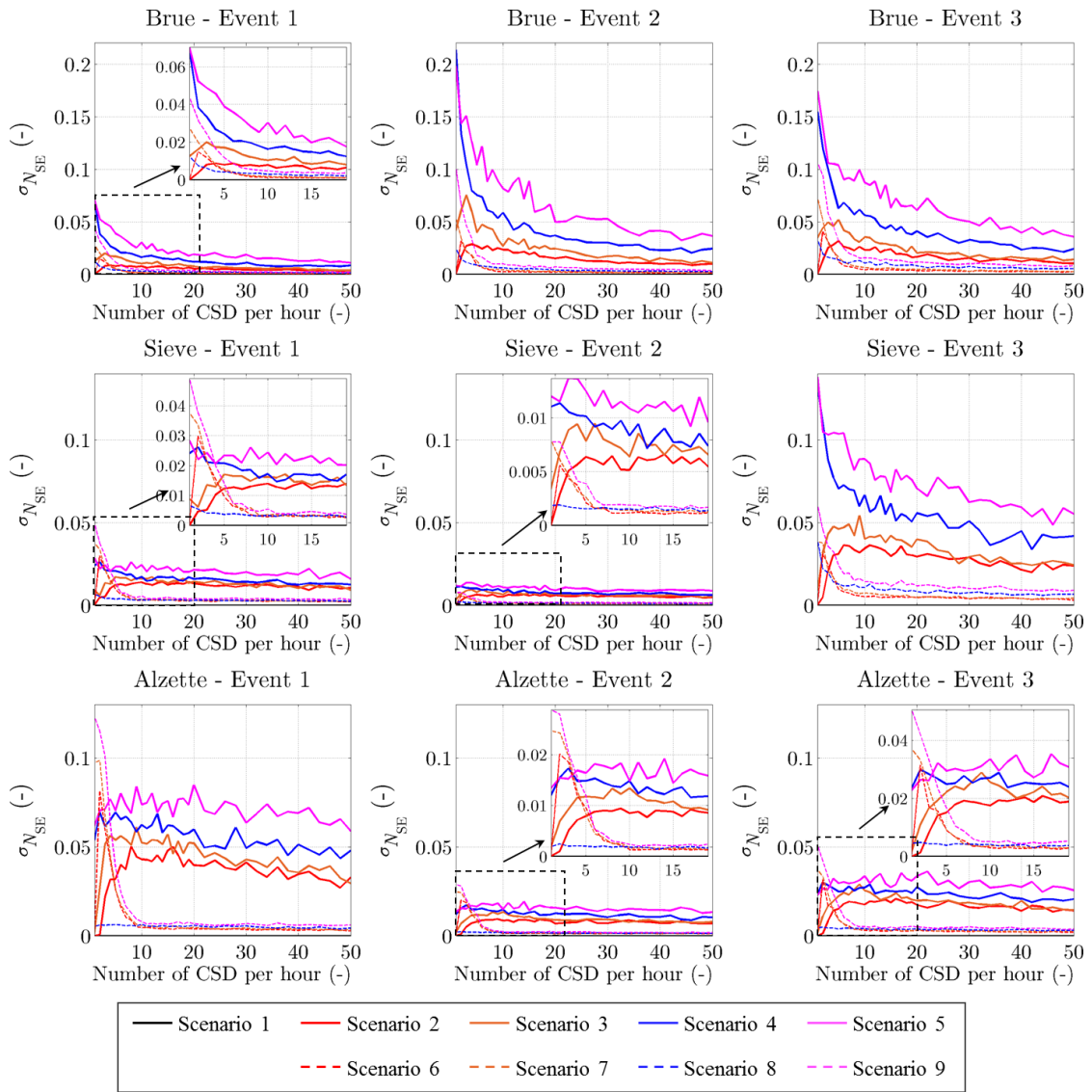
1040



1041

1042 Figure 9. Dependency of the mean of the Nash-Sutcliffe efficiency sample, μ_{NSE} , on the number
 1043 of streamflow crowdsourced data, in the 1 to 9 experimental scenarios for the considered flood
 1044 events, in the three catchments: Brue (upper row), Sieve (middle row) and Alzette (bottom row).

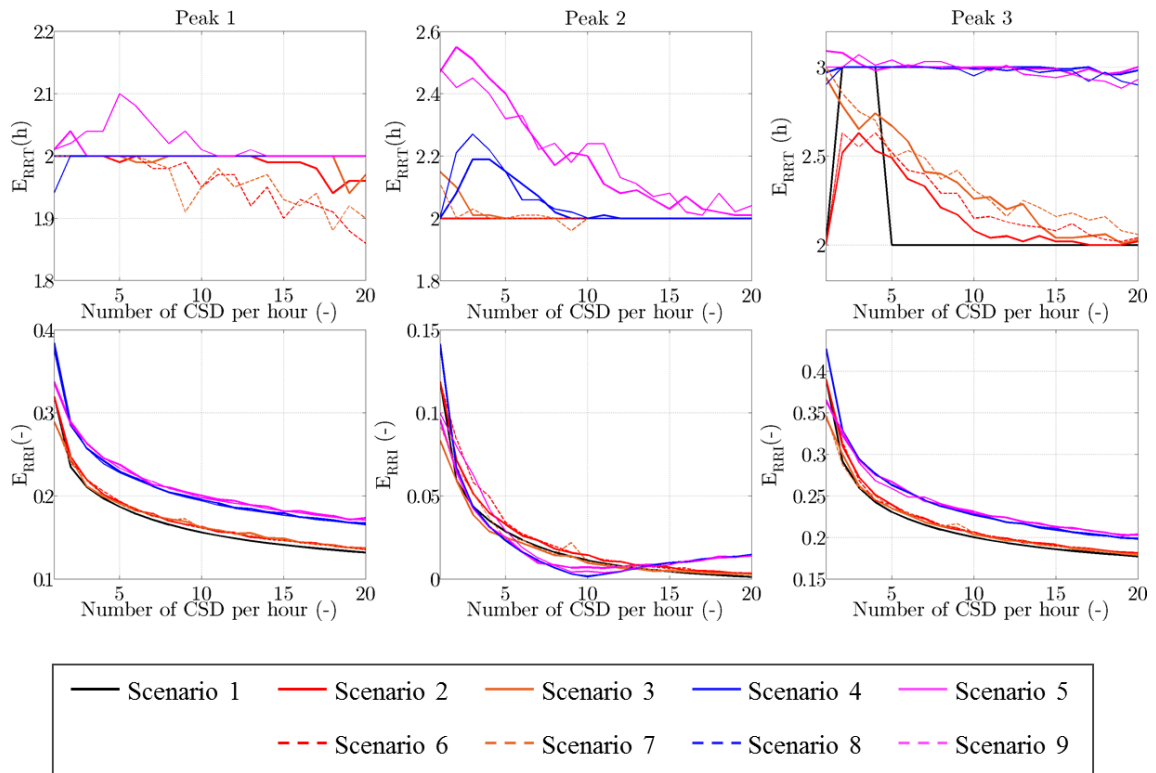
1045



1046

1047 Figure 10. Dependency of the standard deviation of the Nash-Sutcliffe efficiency sample, $\sigma_{N_{SE}}$
 1048 , on the number of streamflow crowdsourced data, in the 1 to 9 experimental scenarios for the
 1049 considered flood events, in the three catchments: Brue (upper row), Sieve (middle row) and
 1050 Alzette (bottom row).

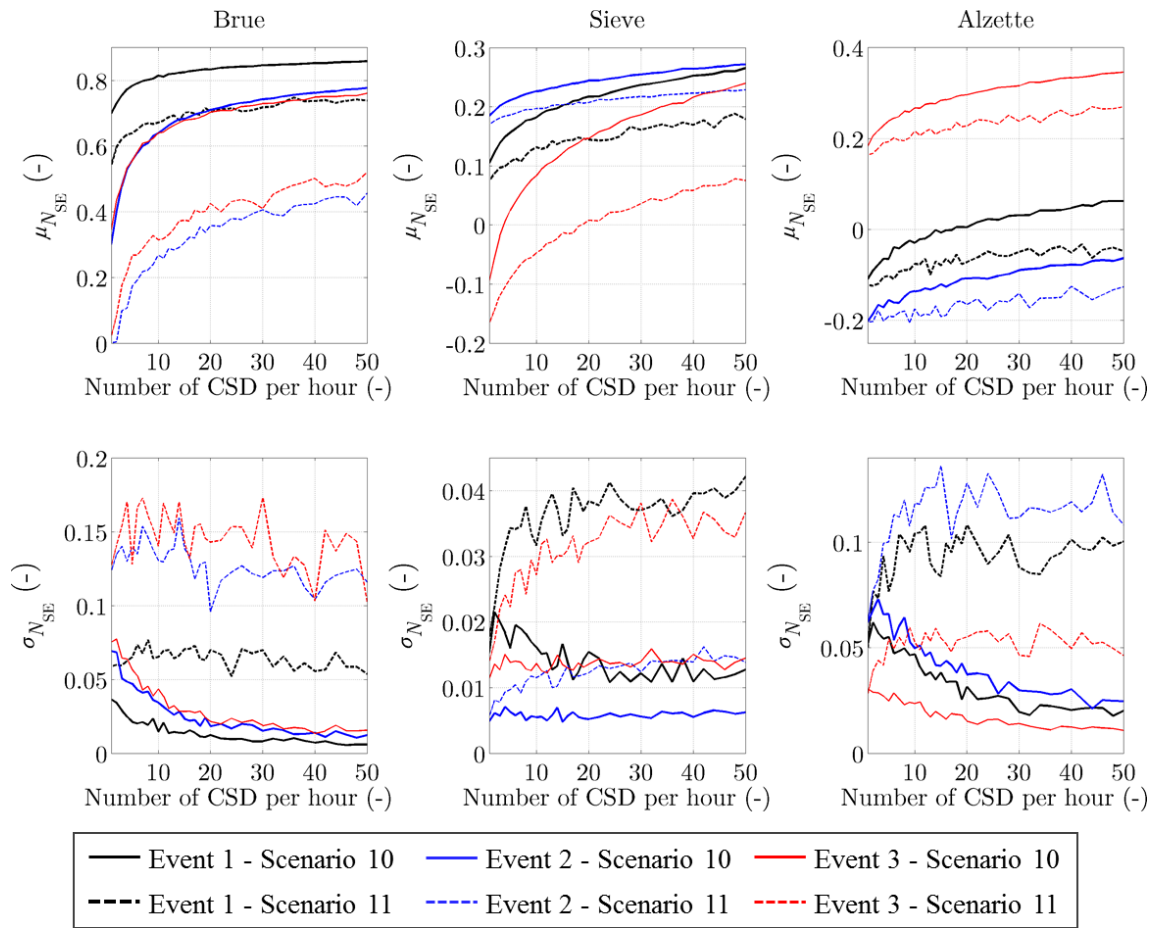
1051



1052

1053 Figure 11. Representation of the errors in flood peak timing, E_{RRT} , and intensity, E_{rri} , (as
 1054 described in Eqs. (20) and (21)), as function of the number of streamflow crowdsourced data
 1055 and experimental scenarios (1 to 9), for three different flood peaks occurred during flood event
 1056 2 in Brue catchment.

1057



1058

1059

1060

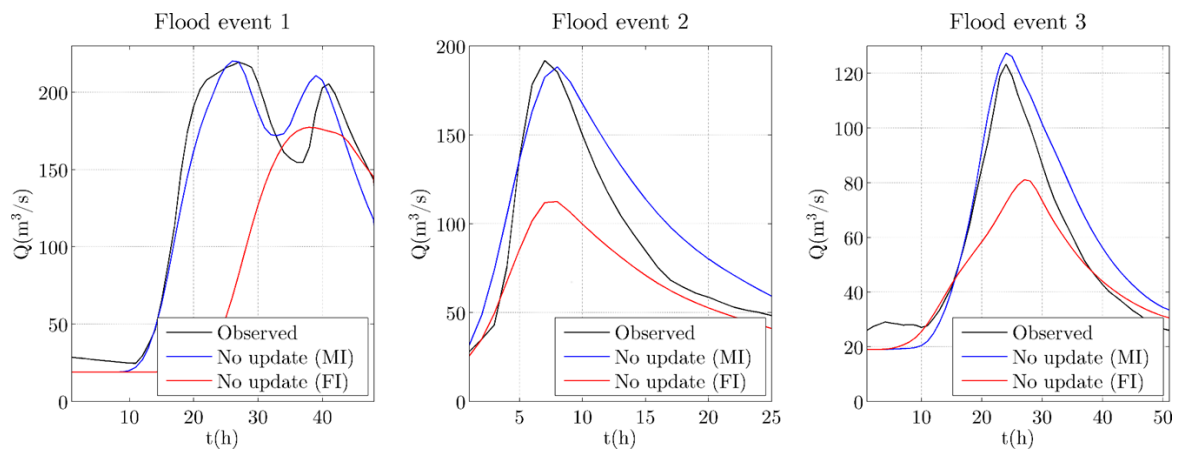
1061

1062

1063

1064

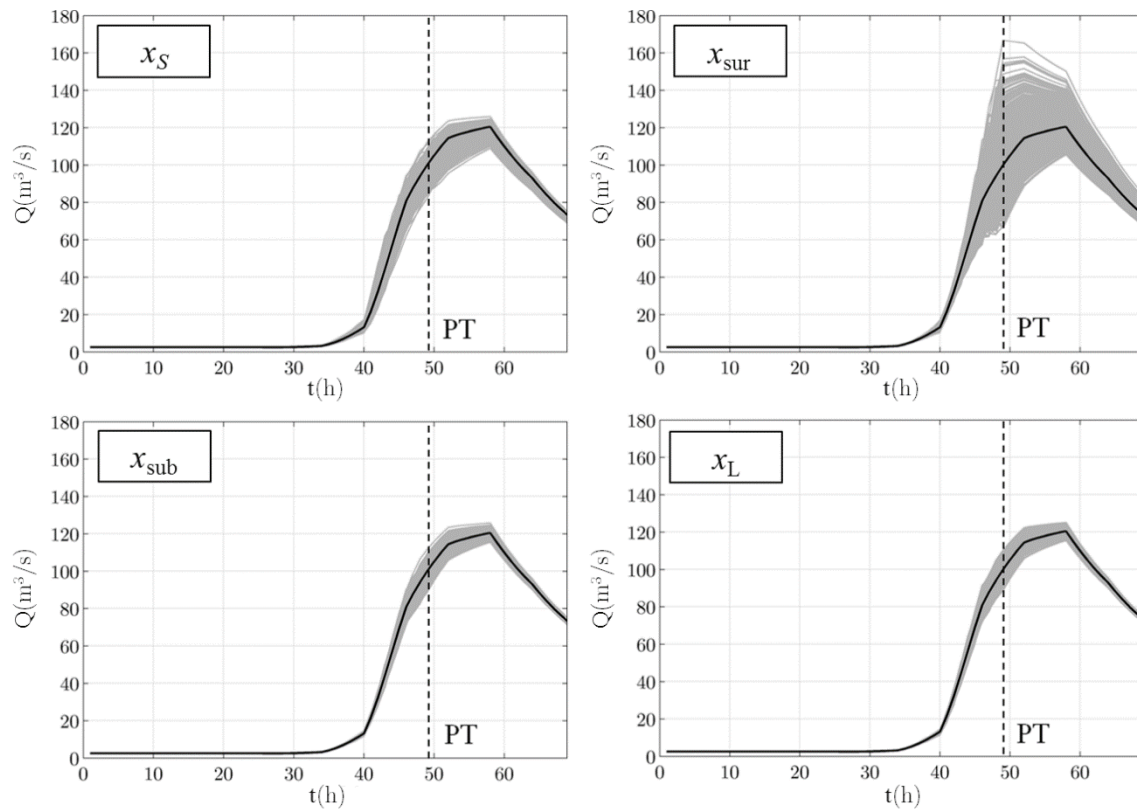
Figure 12. Dependency of the mean $\mu_{N_{SE}}$ and standard deviation $\sigma_{N_{SE}}$ of the Nash-Sutcliffe efficiency sample (first row and second row, respectively), on the number of streamflow crowdsourced data, in the 10 (solid lines) and 11 (dashed lines) for the considered flood events (black, blue, red lines), in the three catchments: Brue (left panel), Sieve (central panels) and Alzette (right panels).



1065

1066 Figure 13. Observed and simulated hydrographs, without update, using measured input (MI)
 1067 and forecasted input (FI), for the three considered flood events occurred in 2013 (event 1), 2014
 1068 (event 2) and 2016 (event 3) on the Bacchiglione catchment.

1069



1070

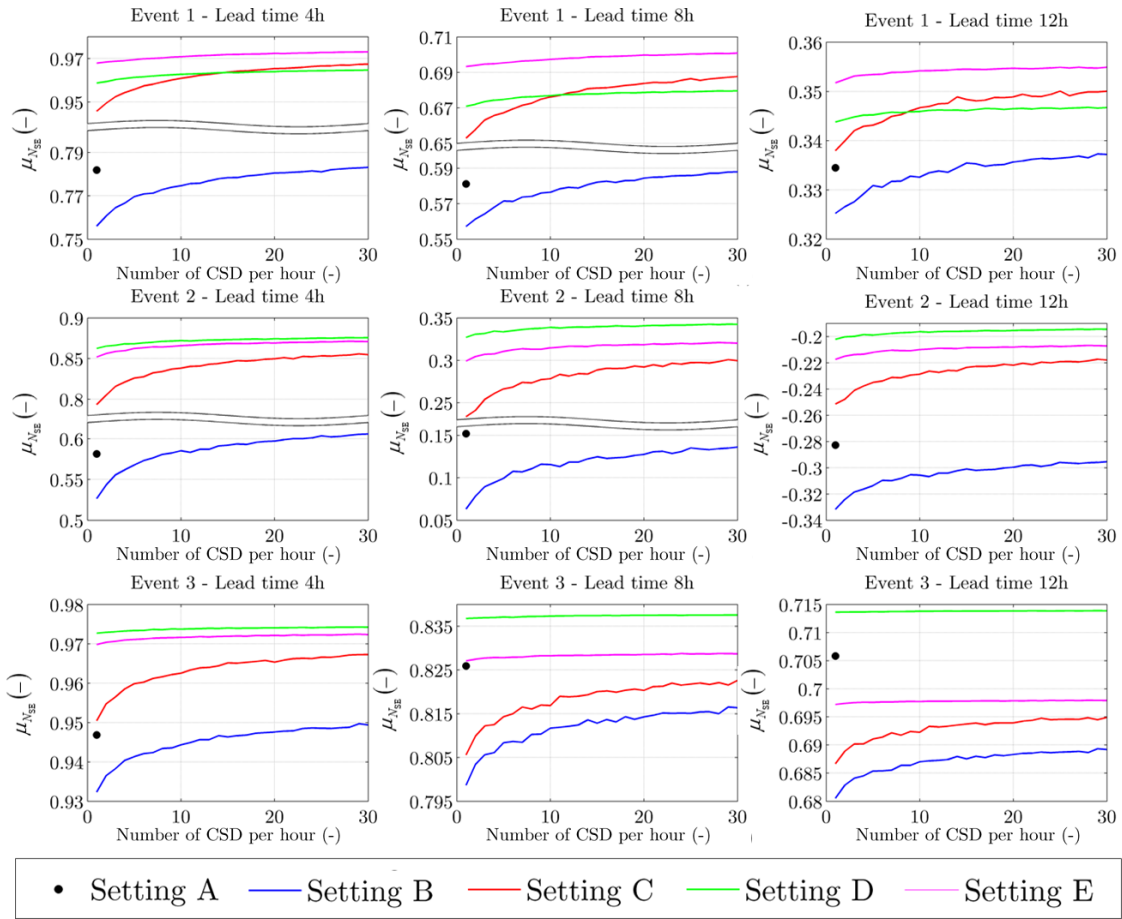
1071 Figure 14. Effect of model state perturbation on the model output for the Bacchiglione

1072 catchment: PT=Perturbation Time; x_S = model state related to S_w ; x_{sur} = model state related to

1073 Q_{sur} ; x_{sub} = model state related to Q_{sub} ; x_L = model state related to Q_g .

1074

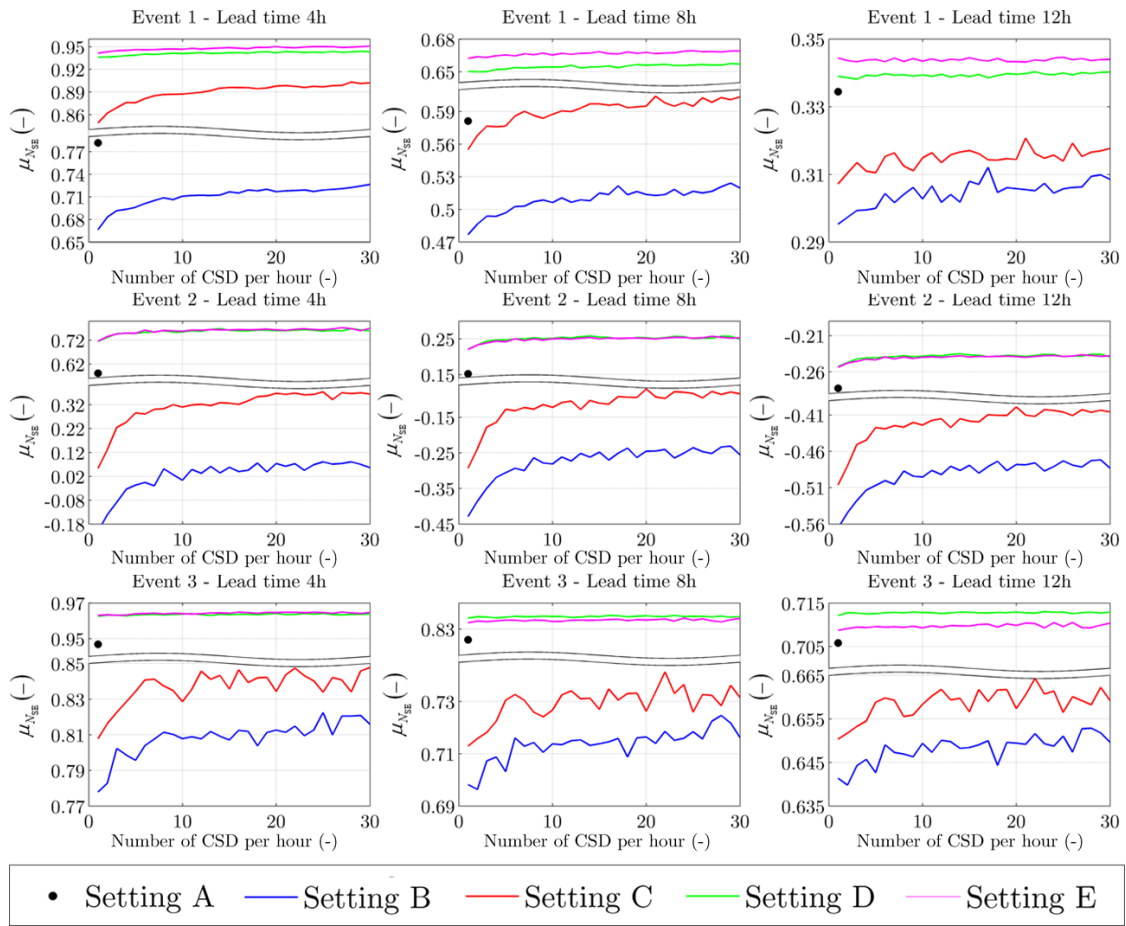
1075



1076

1077 Figure 15. Model performance expressed as mean of the Nash-Sutcliffe efficiency μ_{NSE} –
 1078 assimilating different number of streamflow crowdsourced data during the three considered
 1079 flood events, for the three lead time values (left panels: 4 hours; central panels: 8 hours; right
 1080 panels: 12 hours), of scenario 10, for the 5 experimental settings A to E on the Bacchiglione
 1081 catchment.

1082



1083

1084

1085

1086

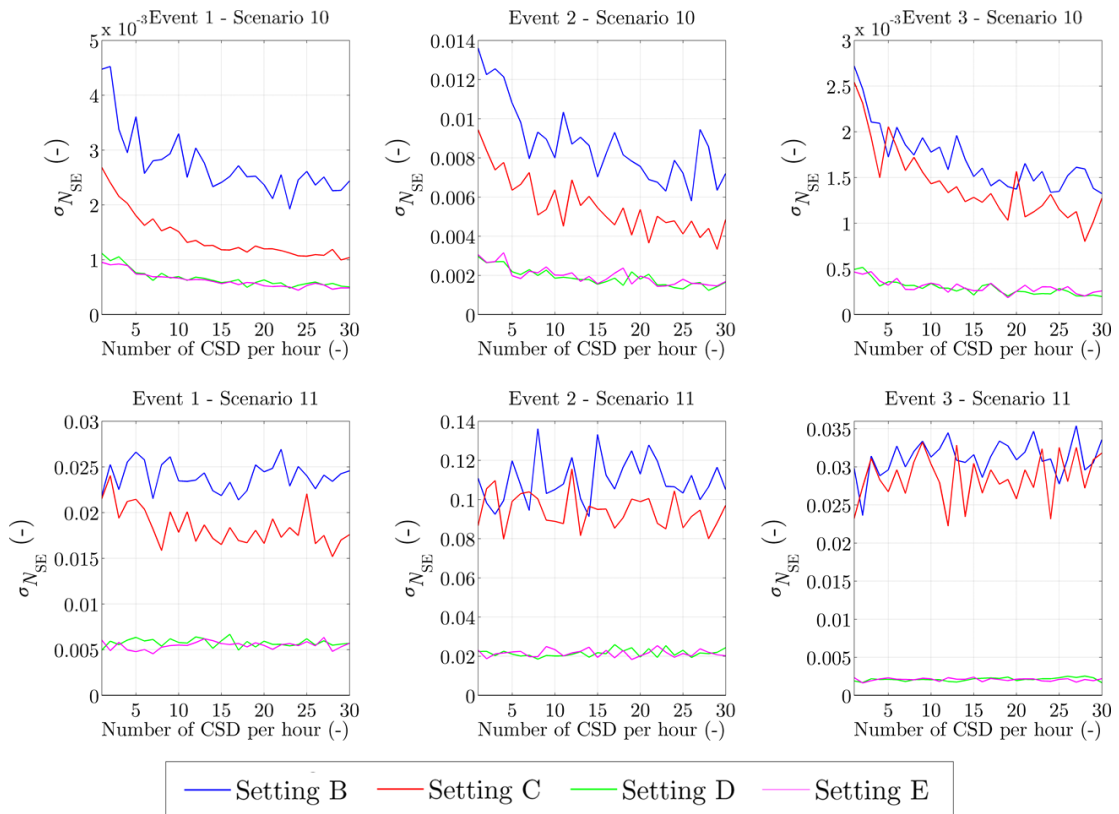
1087

1088

1089

1090

Figure 16. Model performance expressed as mean of the Nash-Sutcliffe efficiency μ_{NSE} – assimilating different number of streamflow crowdsourced data during the three considered flood events, for the three lead time values (left panels: 4 hours; central panels: 8 hours; right panels: 12 hours), of scenario 11, for the 5 experimental settings A to E on the Bacchiglione catchment.



1091

1092

Figure 17. Variability of model performance expressed as $\sigma_{N_{SE}}$ – assimilating streamflow
 crowdsourced data within settings A, B, C and D, assuming lead time of 4h, for experimental
 scenarios 10 (upper row) and 11 (bottom row), during the three considered flood events on the
 Bacchiglione catchment.

1096

1097

1098